MAPPING BIOLOGICAL SOIL CRUST COVER IN THE KAWAIHAE WATERSHED

A THESIS SUBMITTED TO THE GRADUATE DIVISION OF THE UNIVERSITY OF HAWAI`I AT HILO IN PARTIAL FULFILLMENT OF THE REQUIREMENT FOR THE DEGREE OF

MASTER OF SCIENCE

IN

TROPICAL CONSERVATION BIOLOGY AND ENVIRONMENTAL SCIENCE

MAY 2019

By

Eszter Adany Collier

Thesis Committee:

Ryan Perroy, Chairperson
Jonathan Price
Sasha Reed

Keywords: sUAS, biocrust, image classification, Kohala, Hawaii, erosion, Pelekane

Acknowledgements

This thesis was made possible through financial support from the Hawai'i Geographic Information Coordinating Council and the Society for Conservation Biology. Access to fieldwork and data analysis equipment was generously provided by the UH Hilo Geography Department and the Spatial Data and Visualization (SDAV) lab.

I would like to sincerely thank my thesis committee for contributing their time and support. Dr. Perroy's guidance and encouragement were central to the successful completion of this thesis and I will always be grateful for his unwavering faith in my capabilities. Dr. Price taught me everything I know about landscape ecology and his wealth of knowledge about a wide variety of topics was invaluable for filling the numerous *pukas* that sprang up during this project. Dr. Reed's expert knowledge of biocrusts, along with her enthusiasm for the project, was key to bringing my ideas to fruition. In addition, I'd like to thank Dr. Rebecca Ostertag and everyone who works to support the TCBES program for their tireless dedication to student mentorship.

For their logistical support during my field work, I'd like to thank Cody Dwight, formerly of the Kohala Watershed Partnership, and Patti Johnson of the Parker Ranch. I'd also like to thank Dr. Corina Cerovksi-Darriau and Dr. John Stock of the United States Geological Survey for their feedback during the initial stages of this project.

In addition, I'd like to thank the following people for generously sharing their knowledge and providing moral support during my research: Timo Sullivan, Kimo Melcher, and my fellow students in the 2017 TCBES cohort. I'd also like to thank my family – Zsuzsa, Istvan, Aniko and Peter – for their lifelong support of my crazy ideas, in grad school and beyond. Finally, I'd like to give special thanks to my husband, David, whose steadfast encouragement and hard work kept our ship afloat while I pursued this thesis.

Abstract

Historical land use patterns on Hawai'i Island have created degraded dryland ecosystems that are at high risk for erosion. In places such as the Kawaihae watershed in leeward Kohala, the impacts of sediment deposition from the watershed have detrimentally affected coastal marine ecosystems by decreasing habitat quality and burying important cultural sites. Due to the extensive and long-term effects of erosion, it is important to understand and protect non-traditional agents that may help to hold sediments in place. Biological soil crusts are communities of photosynthetic microorganisms that grow over mineral soil in arid and semi-arid ecosystems and are known to increase soil stability. Despite their potential to mitigate erosion, the distribution of biocrusts in degraded drylands on Hawai'i Island is unknown. We mapped biocrusts in the Kawaihae watershed, a semi-arid landscape prone to erosion, using imagery collected by small unmanned aerial systems (sUAS) at three spatial resolutions (1.15, 2.05 and 2.80 cm/pixel). Using a pixel-based methodology, we produced classifications with overall accuracies ≥85% at all three resolutions. As biocrust development is associated with increasing soil stability, we also explored this relationship in the Kawaihae watershed. We identified 3 different biocrust levels of development (LOD) and conducted soil aggregate stability testing at all development levels. We found that there was a significant increase in soil stability between soils without surface biocrusts (LOD score of 0) and those with biocrusts at any development level (LOD 1-3). More highly-developed biocrusts imparted greater soil stability than less-developed biocrusts, but the impact on soil stability reached a ceiling beyond biocrust LOD 1. In addition, we applied our mapping methodology to investigate the direct impacts of biocrusts on soil loss. We overlaid our classified maps with digital surface models (DSMs) from data sets covering a 2.75-year time span. We found trends of varying soil loss between biocrust and bare soil areas, but more field work is needed to verify our results. We also explored the effects of grazing animals on biocrust cover by comparing classified images of a grazed site and a grazing-exclusion site. We found differences in biocrust coverage between the sites, including differing proportions of the land cover types present, but additional field data collection is necessary prior to drawing definitive conclusions. Overall, our project provides a new biocrust mapping methodology that could be used by researchers and land managers globally and adds insight into the role of biocrusts in erosion prevention in the Kawaihae watershed and similar arid/semi-arid landscapes.

Table of Contents

List of Tables

List of Figures

List of Abbreviations

AGL: above ground level

DN: digital number

DSM: digital surface model

GCP: ground control point

LOD: level of development

PA: producer accuracy

ROI: region of interest

sUAS: small unmanned aerial systems

UA: user accuracy

Chapter 1: Introduction

Drylands, which include arid and semi-arid landscapes, are one of the major ecosystems on Earth and encompass nearly half of the planet's terrestrial surface. Characterized by limited water availability and often intense temperatures, drylands exhibit a patchy vegetation distribution (Meron et al. 2007) with areas of exposed soil susceptible to erosive forces. Precipitation in drylands is sporadic; extended dry periods are often followed by short-lived but intense precipitation events (Noy-Meir 1973, Sala & Lauenroth 1982). High-intensity rainfall events readily transport sediments (Nearing et al. 2005) and are associated with higher erosion severity (Wei et al. 2009). Erosion is detrimental to a wide variety of ecosystem processes, ranging from nutrient cycling (Quinton et al. 2010) to climate change resilience (Lal 2004), making it an important topic for conservation research.

The island of Hawai'i contains semi-arid landscapes along its western, leeward side. Several mountainous peaks block easterly trade winds, limiting precipitation across the west side of the island (Kidd & McGregor 2007) and promoting more arid ecosystems. The Kawaihae watershed, located on the western slope of Kohala volcano, is one of these ecosystems (Figure 1-1). Precipitation varies along an elevational gradient but most of the Kawaihae watershed sees less than 500mm of rain per year (Giambelluca et al. 2013) and is therefore considered to be a semi-arid landscape (Noy-Meir 1973). Vegetation also varies along an elevational gradient, but in the semi-arid areas the land cover consists primarily of grasses, such as introduced buffel and guinea grasses, as well as native *pili* grass (Stewart 2005). Although there are several gulches, there are no perennial streams except at the upper reaches of the watershed (Stewart 2005). Soils are primarily silt loam or sandy loam, with varying amounts and sizes of rocks, on a bed of `a`a lava flows (Sato et al. 1973, Natural Resource Conservation Service 2013).

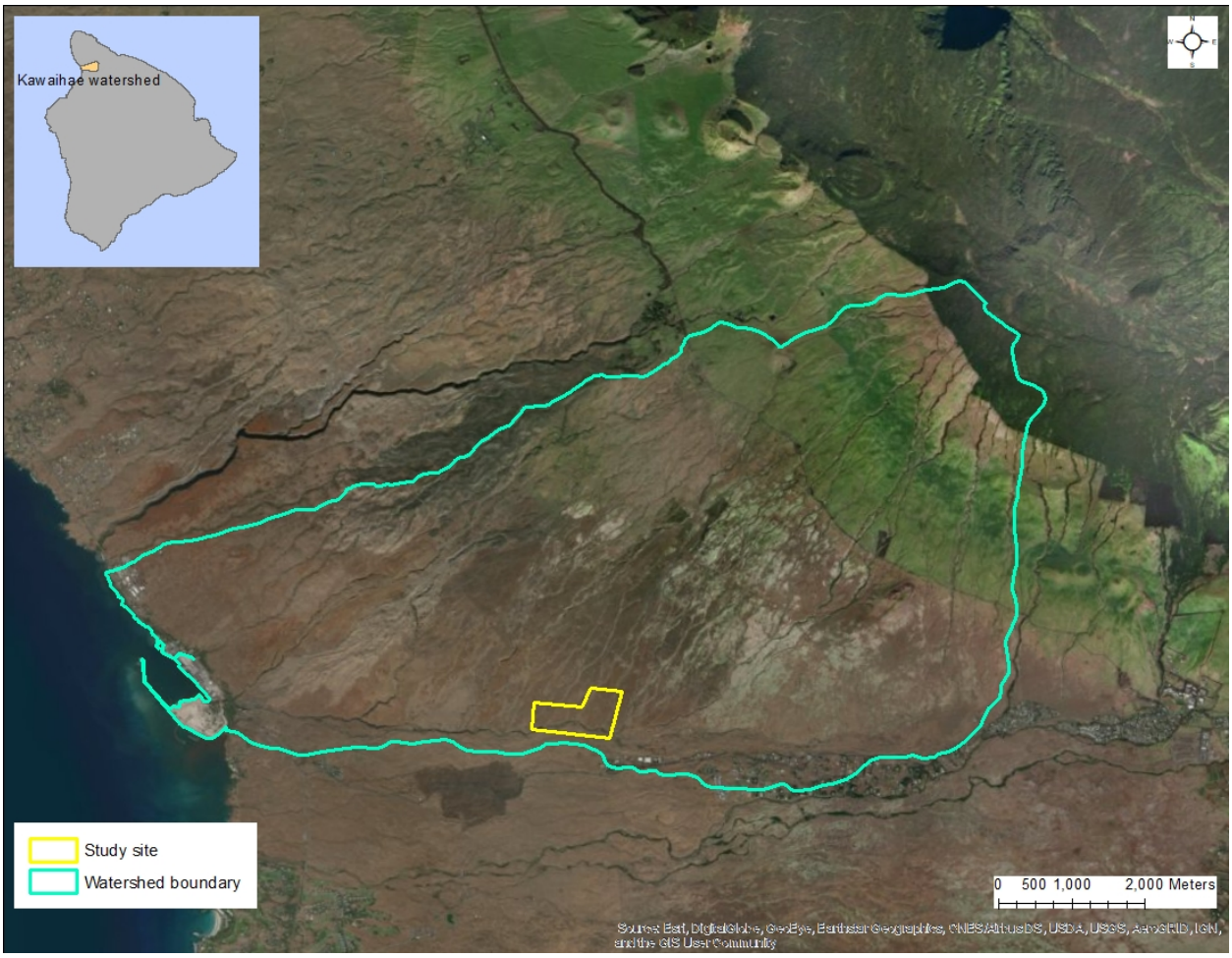

Figure 1-1: Map showing study area within Kawaihae watershed. Inset map shows location of watershed relative to Hawai'i Island.

Originally sandalwood-dominated forest that stretched almost completely down to the coast, most of the watershed was cleared in the 1800s and subsequently used for pasture (Greene 1993). The dual impacts of tree loss and livestock grazing have left large parts of this landscape at high risk for erosion, with an average estimated rate of 4,222 tons of sediment loss per year (Oceanit Center 2007). The landscape of the Kawaihae watershed exhibits erosion rills created by ephemeral streams that form during storm events (Stewart 2005), which in turn create prime locations for sediment transport downhill (Lal 1990). Loss of sediments causes the loss of parent material and nutrients necessary for plant growth (Verity & Anderson 1990; Pimentel et al.

1995), which further inhibits vegetation cover and can cause a positive feedback cycle which exacerbates erosion.

Erosion within the Kawaihae watershed is of concern beyond the terrestrial effects of soil loss. Water in the Pelekane Bay, located at the mouth of the watershed, is so turbid that the bay is listed as an 'impaired water body' by the U.S. Environmental Protection Agency (Hawaii State Department of Health 2014). Much of the sediment loss occurs during rare storm events, but as climate change causes storms in the Hawai'ian Islands to become more intense (Timm & Diaz 2009), the erosion rate has the potential become even higher. The watershed's outlet is adjacent to a coral reef ecosystem, and sediment deposition into the marine environment (coupled with the construction of Kawaihae harbor) has been linked to a 44% decrease in coral abundance and a re-structuring of the benthic coral community in Pelekane Bay (Stender et al. 2014). Coral recruitment has also been shown to be lower in parts of the bay that are more heavily impacted by sediments (DeMartini et al. 2012) and sediment deposition has had a detrimental impact on the abundance of aquatic invertebrates (Tissot 1998). In addition, Pelekane Bay is known historically to be the location of *Hale o Kapuni Heiau*, a native Hawai'ian temple dedicated to shark gods (Cheney et al. 1997). The exact location of the temple within that bay is unknown, however, because sediment transported down from the watershed has completely buried this important cultural site (Cochran et al. 2006).

Several terrestrial conservation initiatives have been implemented as a response to the poor water quality of Pelekane Bay. One strategy has been to install check dams that collect eroding soil and prevent it from entering the bay (Moss 2011). To maximize their soil collection capability, optimal placement of sediment check dams is highly important (Polyakov et al. 2014). Placement of dams is based, in part, on an identification of areas that are at high risk for erosion. An erosion risk assessment has been performed in the watershed, but this assessment identified areas of high sediment movement that are as much as 300m wide (Oceanit Center 2007) which is too generalized to identify optimal placement of ~5m-wide check dams. Another strategy used to mitigate erosion in the watershed has been to out-plant native grasses to help stabilize soils. However, this option is time-consuming and expensive because out-planting requires investment in seedlings and labor to plant them. In addition, the dry climate of the Kawaihae watershed necessitates irrigation until plants can become established (Stewart 2005), which increases costs

further. These efforts have been credited for improvements such as increased fish populations between 1996 and 2014 (Stender et al. 2014), but the sediment in Pelekane bay is still mostly of terrestrial origin (Takesue & Storlazzi 2019), indicating that sediment loss from the Kawaihae watershed is an ongoing problem.

Considering the long-lasting impacts of erosion in the terrestrial and marine ecosystems, other factors that may help mitigate soil loss should be investigated. In many arid and semi-arid regions bare soil is often covered by biological soil crusts, often referred to as "biocrusts". Biocrusts are communities of microorganisms (Figure 1-2) that grow in the topmost layers of soil (Rosentreter et al. 2007). Biocrust species composition varies under different environmental conditions (Bowker et al. 2018), but some of the dominant organisms are cyanobacteria, lichen, and mosses (Belnap et al. 2001). Biocrust development generally occurs in stages with visually observable development levels. The earliest development level is dominated by cyanobacteria, which are able to establish colonies on bare soil (Budel et al. 2016) and are either very difficult to see with the eye or exhibit a dark brown-to-black color. The next development level is the lichen-dominated stage, characterized by patches of lichen thalli, and the third development level is moss-dominated, which appears as light or dark green (Seppelt et al. 2016). Development level and associated community composition is dependent, however, on factors such as climate and soil texture (Fischer & Subbotina 2014), as well as physical disturbance (Kuske et al. 2012).

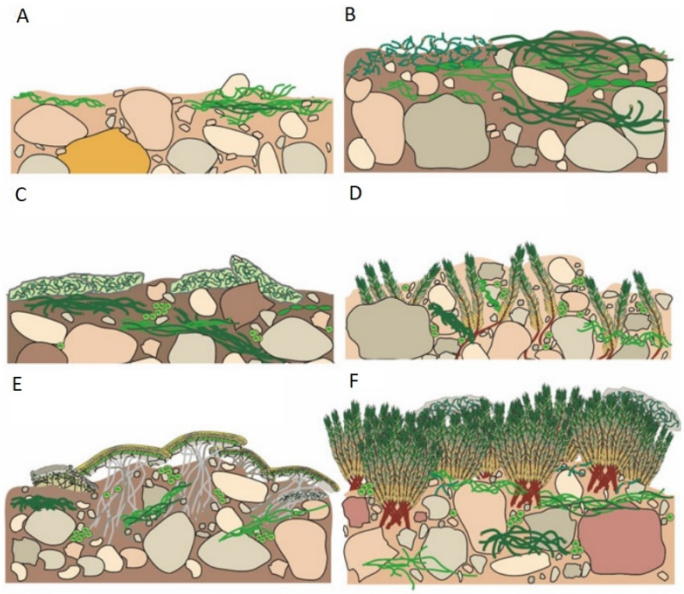

Figure 1-2: Cross-sectional diagram of a typical biocrust, showing progression (A-F) from initial colonization (A) through late-stage development (F). *note: figure is not drawn to scale. For reference, a typical biocrust extends ≤5mm below the soil surface (image: Colesie et al. 2016).

Although found in a variety of ecosystems, biocrusts are most common in semi-arid and arid landscapes because they are able to survive very low water availability (Belnap et al. 2001), which inhibits the growth of vascular plants. In these ecosystems, biocrusts perform many of the important functions typically associated with plants, including enhancing soil aggregate stability and reducing erosion (Belnap et al. 2001, 2003). Cyanobacteria-dominated biocrusts are known to develop filaments (Figure 1-3) that act as a glue to hold soil particles together (Belnap & Gardner 1993). Previous research has found that biocrust biomass has a positive relationship to soil stability (Bowker et al. 2006, Belnap et al. 2008), but the site-specific development of biocrusts means that their relationship to soil stability may differ among landscapes.

Figure 1-3: Scanning-electron micrograph of filamentous cyanobacteria. Filaments are visible as hair-like structures wrapping around the soil particles (image: USGS).

Research has not been conducted on biocrusts distribution or overall function in Hawai'i, though there have been species-level studies focused on mosses and lichens (Crosby 1965, Smith 1981, Staples 2004, Jorge-Villar & Edwards 2008). Thus, the relationship between biocrusts and soil stability, specific to Hawai`i, remains unknown. Considering their erosion-mitigating potential, knowledge of biocrusts and their associated soil stability would be beneficial for land managers and conservation researchers working in Hawai'ian drylands. Our research explores the impacts of biocrusts and their development on the aggregate stability of soil the Kawaihae watershed. Soil aggregate stability is a reliable indicator of erosion risk (Barthes & Roose 2002), so a greater understanding of this relationship may assist research and conservation in the watershed as well as other arid and semi-arid landscapes in Hawai`i.

The erosion risk assessment that was previously performed for the Kawaihae watershed did not consider biocrusts and was limited in its spatial resolution of land cover to 30 m satellite imagery (Oceanit Center 2007). Biocrusts distribution can vary on a micro-scale (within a few

meters) (Bowker et al. 2006), so maps generated from large-scale data will likely overlook this important soil stabilizer. However, recently-developed remote sensing technologies such as small Unmanned Aircraft Systems (sUAS) can produce high-resolution images useful for investigating biocrust distribution in great detail. sUAS platforms have successfully been used to map a variety of land cover types via image classification (Yu et al. 2006, Michez et al. 2016, Mafanya et al. 2017, Duffy et al. 2018), but to our knowledge have yet to be used for classifying biocrust cover. Past remote sensing studies on biocrusts have been limited to coarse-resolution, multi- and hyperspectral approaches (Karnieli et al. 1997, Chen et al 2005, Rodriguez-Caballero et al. 2014, Rodriguez-Caballero et al 2017, Rozenstein & Adamowski 2017), which involve costly equipment and complex calibration and processing methods. Our research aimed to develop a classification technique for biocrust cover from commercially-available sUAS platforms and visible wavelength cameras. The development of such a methodology would allow biocrust researchers without access to specialized geospatial equipment to generate highly-detailed biocrust distribution data at small spatial scales and would open the doors for further study of biocrust characteristics and functions.

In addition to developing a mapping methodology, our research applies classified maps generated from sUAS data sets to an investigation of the influence of grazing animals on biocrust cover. This research topic is important for conservation efforts because the Kawaihae watershed is currently managed for ranching as well as restoration. Cattle can have a detrimental effect on biocrusts through trampling, which reduces biocrust coverage (Kuske et al. 2012, Concostrina-zubiri et al. 2014). However, the effect of grazing ungulates on biocrust cover in the Kawaihae watershed is unknown due to the variability in biocrust formation between landscapes and the overall lack of knowledge about biocrusts in this area. An investigation of the relationship between grazers and biocrusts in this ecosystem is important to gain an understanding of the nature of biocrust distribution across the landscape and a deeper knowledge of the impacts of cattle ranching in the Kawaihae watershed.

We also extend our research to the connection between biocrust distribution and erosion by directly measuring soil loss under different land cover types using sUAS-derived data sets that span several years. The sUAS platform is well-suited for structure-from-motion photogrammetry, which is a method to construct three-dimensional elevation and surface models

from overlapping images taken at multiple angles (Westoby et al. 2012). Digital elevation models (DEMs) and digital surface models (DSMs) can be created with structure-from-motion algorithms using images collected by sUAS (Turner et al. 2012) and have been shown to be comparable to traditional topographic survey methods (Tonkin et al. 2014, Cook 2017). Biocrust topographical characteristics that are related to erosion have been explored with high-resolution DEMs (Rodriguez-Caballero et al. 2013), but this research was limited to plot-level data sets and did not measure soil loss. Our research uses structure-from-motion methodology to measure the spatial distributions of soil loss relative to ground cover type, which can provide more insight on the relationship between biocrusts and erosion.

Biocrusts have been referred to as "diminutive communities of potential global importance" (Ferrenberg et al. 2017). Our research seeks to expand the knowledge base of these communities by developing a research tool for future biocrust and dryland studies, and by providing insight into the relationship between erosion and biocrusts in Hawai'ian drylands. In the following chapters, we describe the development of our mapping technique and how we have applied it to research questions regarding erosion and land use in the Kawaihae watershed. We interpret our results within the context of the watershed and discuss their implications for conservation in this ecosystem, as well as other drylands in Hawai'i and beyond.

Chapter 2: Mapping biocrusts with sUAS imagery

2.1 Introduction

Biocrust distribution can vary at very small spatial scales (Bowker et al. 2006), which creates limitations for traditional remote sensing mapping approaches that use conventional, satellite-derived data sets. Consequently, the use of very high-resolution imagery to map spatial distribution has been identified as a priority in the field of biocrust research (Belnap et al. 2016). Our objective was to use the sUAS platform, which has been shown to be useful for classifying many different land cover types (Andersen & Gaston 2013), to create classified biocrust maps. Previous remote sensing classifications of biocrusts have relied on hyperspectral data (Rodriguez-Caballero et al. 2014; 2017), but we were interested in exploring the use of platforms outfitted with cameras operating within visible wavelengths (RGB). In this way we tested the feasibility of using relatively inexpensive, commercially-available equipment for biocrust mapping.

We first assessed the fundamental ability of the classification scheme to distinguish biocrusts and bare soil within non-vegetation areas. We also assessed the ability of the classification algorithm to distinguish between biocrusts at different stages of development. Biocrust morphology and color changes as biocrusts develop across successional frameworks, creating subtle but visibly-distinct differences among development levels (Colesie et al. 2016). Although we recognized that this would be a challenge with solely visible-wavelength imagery, we hypothesized that the classification algorithm would be able to distinguish between varying development levels because differentiation between land cover types with similar spectral characteristics has been shown to be possible using sUAS platforms (Ventura et al. 2016, Gomes et al. 2018). The purpose of differentiating biocrust levels of development was to link the classified images to soil stability field data (see section 3.3) and to determine if biocrusts can be mapped as an indicator of relative soil stability and erosion risk.

We also investigated the impact of increasing spatial resolution on classification accuracy by collecting aerial data at three different altitudes above ground level (AGL). We hypothesized that as spatial resolution decreased, the classification accuracy would also decrease, which is consistent with previous research comparing spatial resolution and classification accuracy of sUAS-derived imagery (Torres-Sanchez et al. 2014, Lopez-Granados et al. 2015). In the

following sections, we present our field data collection and data analysis methods, as well as the results and a discussion of this research.

2.2 Methods

Creating classified maps of biocrust distribution involved collecting and processing aerial images. Prior to collecting complete sUAS image data sets over the study area, we experimented with camera settings and lens filters to optimize image quality. Aerial data were then collected under these optimized parameters and processed to generate mosaics which were used for subsequent image classification.

2.21 Study site

As introduced in Chapter 1, the Kawaihae watershed is located on the leeward (west) side of Kohala Mountain (inset, Figure 1-1) on the island of Hawai`i. The watershed is bound on its south side by state highway 19, on its north side by Makahuna Gulch, and extends from sea level to 1645 m elevation, encompassing an area of 50 km² (Stewart 2005). The study site sits within the watershed at an elevation of 1200m and is dominated by patches of grasses and shrubs interspersed with exposed ground. The study site was selected based on preliminary observations of biocrust presence as well as the designation of the site as especially high-risk for erosion, relative to other sections of the watershed (Oceanit Center 2007).

2.22 sUAS flights

All missions were flown with a DJI Inspire 2 platform outfitted with an X5s camera (DJI, Shenzen, China). Prior to conducting flights, we placed three calibration tarps (Group VII Technology, Provo, Utah) with uniform reflectance values (0.03, 0.35, and 0.56) within the center of the flight area to provided standardized reference data for the different flights (Figure 2-1). During preliminary flights for this research, we observed considerable solar artefacts (Figure 2-2A) on the mosaics generated from flights conducted in our study area. These artefacts arise from variable brightness across the individual raw images that compose the mosaic (Figure 2-2B, see section 2.13 for a description of image processing) and are a common problem for sUAS-derived imagery collected under full-sun conditions (Garaba et al. 2012, Ortega-Terol et al 2017). Prior to conducting sUAS flights for data collection, we conducted a set of informal

experiments to find the optimal set of camera and flight parameters that would eliminate these artefacts from our imagery.

Figure 2-1: Calibration reflectance tarp, as seen in the mosaic generated from the 40 m AGL flight. Reflectance values (L-R): 0.03, 0.35, 0.56.

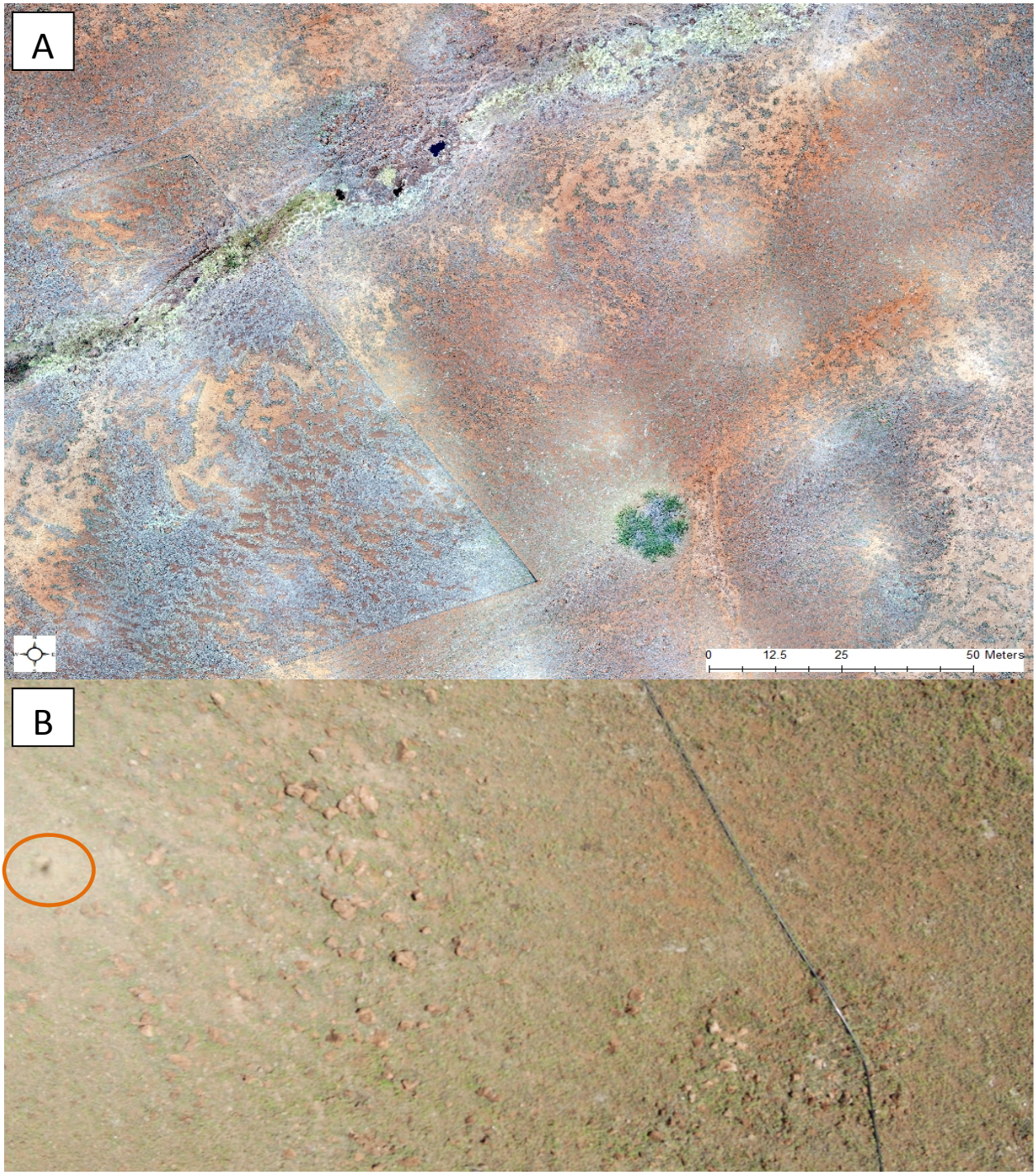

Figure 2-2: (A) Map showing solar artefacts visible bright spots across imagery. (B) Raw sUAS image showing higher brightness on left side of image than on right (drone shadow visible in orange oval).

We identified camera exposure settings and the use of lens filters as possible solutions and tested these parameters by conducting flights in September, 2018, using two complementary sUAS mapping applications: DJI Go (DJI, Shenzen, China) and Maps Made Easy (Drones Made Easy, San Diego, CA). Maps Made Easy can perform automated flights with line or grid patterns (DJI Go flies in manual mode only), and DJI Go has multiple camera exposure settings (Maps Made Easy only offers automatic exposure). We compared two exposure settings: automatic (exposure self-adjusts based on the camera's internal light meter), and locked (exposure manually set prior to flight and does not change during flight) (Table 2-1A). The exposure lock was set while hovering over the calibration tarp prior to collecting images.

Table 2-1: flights conducted with (A) various exposure settings and (B) different lens filters.

						Adjusted Parameters	
	Mapping App	Flight	Altitude (m)	Flight Pattern	overlap	Exposure	Lens Filter
A	DJI Go	1EXP	20	Line	NA	Automatic	NA
		2EXP	20	Line	NA	Auto-locked while hovering over calibration tarp	NA
B	Maps Made Easy	1FLTR	40	Grid	85/85	Automatic	Polarized
		2FLTR	40	Grid	85/85	Automatic	ND8 + polarized (ND8/P)
		3FLTR	40	Line	85/85	Automatic	ND16 + polarized (ND16/P)

To test the effects of filters, we used neutral-density and polarized lens filters (Table 2-1B), chosen from a set (PolarPro, Los Angeles, CA) that fit over the camera lens. Neutral density (ND) filters are similar to sunglass shades and filter out incoming light to create images that have lower overall brightness. The number associated with the filter indicates the light-filtering intensity; a higher value equates to less light reaching the sensor. Polarized (P) filters limit incoming light to one direction, eliminating scatter and lowering glare. In addition, these two filter types can be combined to create an additive effect.

We also considered different flight patterns as possible solutions, based on our familiarity with the mosaic-generation process. Maps Made Easy provides options for two flight patterns, line and grid (Figure 2-4). Line flight patterns provide across track and along track image overlap, but the grid pattern allows for more overlap by creating a larger image set.

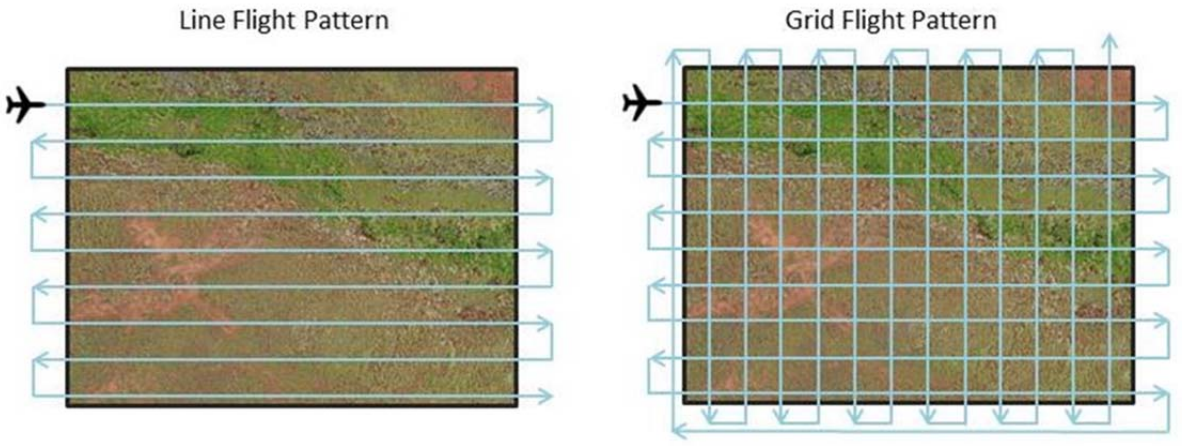

Figure 2-3: Diagram of line (left) and grid (right) flight patterns.

Test flights were conducted at 20 m or 40 m AGL under sunny skies in an area adjacent to our study site with the calibration tarp placed in the center of the flight extent.

Based on the results of these test flights (see section 2.21), all data collection missions were flown in the presence of the calibration tarp with a line flight pattern under uniformly overcast skies or within 10 minutes of sunrise (during which time incoming sunlight was shaded by mountains) and without lens filters. We also set the camera white balance to “sunny”, which is an internal setting that prevented the white balance from shifting in response to the aircraft collecting images over the calibration tarp. To compare spatial resolution and image classification accuracy, we conducted flights in October 2018 at three different altitudes: 40 m, 80, and 115 m (115 m being proximal to the maximum FAA-allowed flight altitude of 400 ft), which corresponded to increasingly coarse spatial resolutions (Figure 2-5).

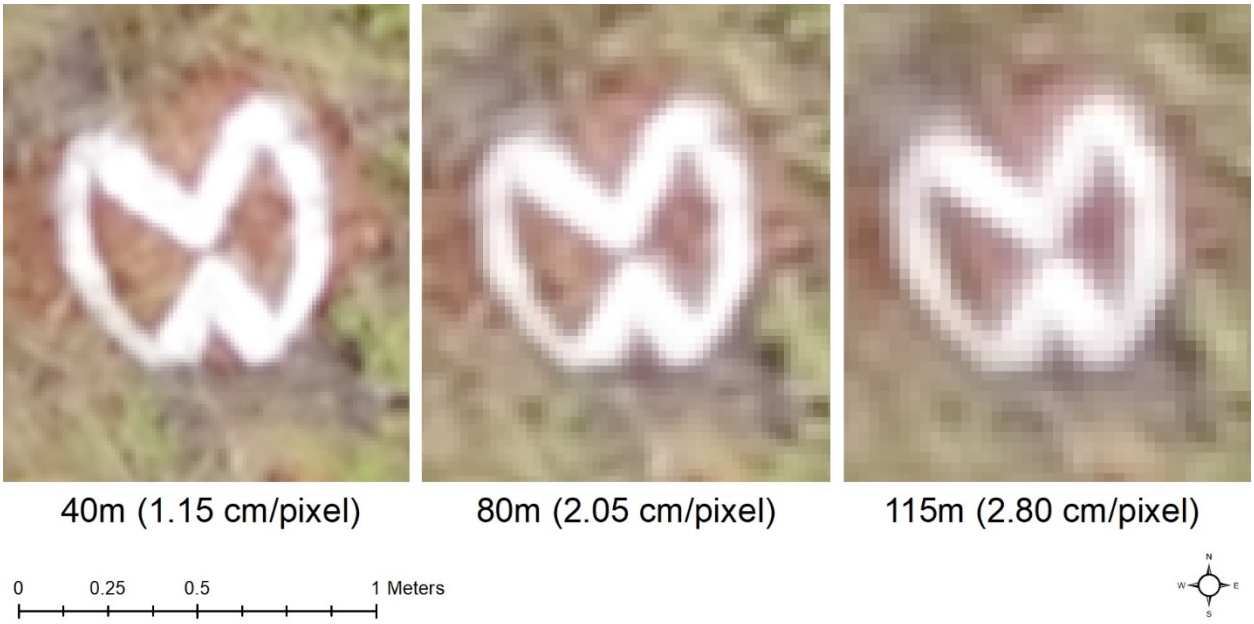

Figure 2-4: Close-up of a GCP from each mosaic. Labels denote sUAS flight altitudes with corresponding pixel sizes in parenthesis.

2.23 Field data collection

Seven ground control points were established by marking immovable, large rocks and then collecting differential GPS (dGPS) positional data over the markings using a Trimble GeoXH unit outfitted with a Trimble Zephyr GNSS antenna (Trimble Inc., Sunnyvale, CA). The occupation time was ~2 minutes for each point which provided a final positional mean root-mean-square error (RMSE) of 1.1cm at 40 m AGL, 1.5cm at 80 m AGL, and 3cm at 115 m AGL, as determined from the results of the incorporation of GCP data during image processing (see section 2.24) .

To assess the effectiveness of test flight parameters on bright spot reduction, we collected soil color field data from within the extent of the area mapped during test flight 3FLTR, the flight that reduced bright spots the most (discussed further in sections 2.21 and 2.31). Soil color was measured using Munsell color notation. The Munsell notation system (Munsell 1919) is widely-used in soil science research and provides a baseline for assessing variable brightness across the imagery. Soil color was measured by collecting a small sample, taking care not to mix

the surface and subsurface components, at 3m intervals along 30 mtransects (Figure 2-5). Transects were oriented to cross the study site at locations where brightness variations were visible in the imagery. Each sample was compared with color chips provided in a Munsell color field guide (Munsell company, New Windsor, NY) to determine soil surface color.

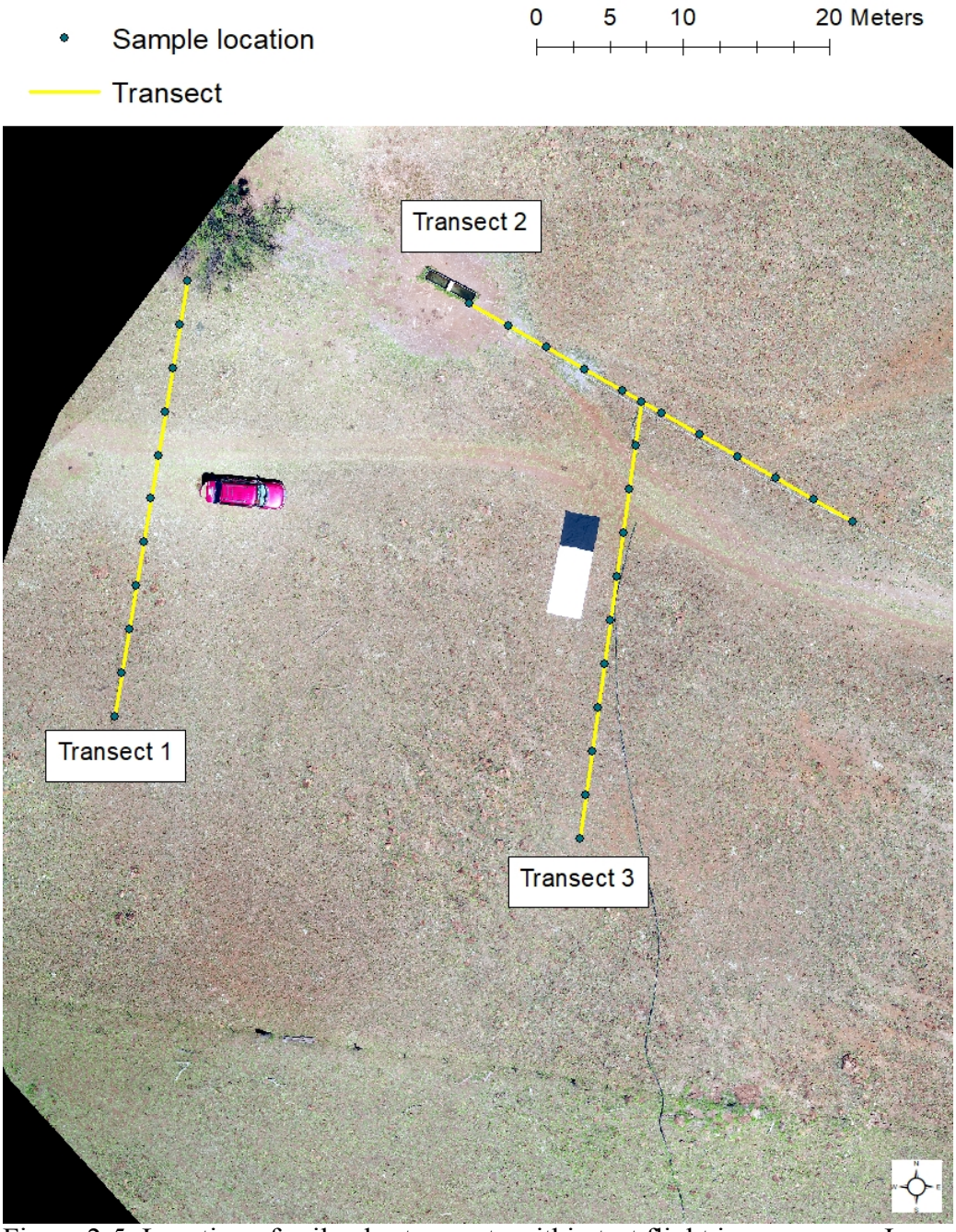

Figure 2-5: Location of soil color transects within test flight imagery area. Image stretch has been adjusted to emphasize bright spots.

To acquire ground truth data for training and validating the image classification scheme, we generated 100 random points across the extent of the processed imagery using ArcMap v 10.4 (Esri, Redlands, CA). Points were located at least 2m from the edge of the imagery, and all points were at least 3m apart (Figure 2-6). The location of each point was then loaded onto Trimble GeoXH handheld GPS units, which were used to navigate to each point in the field. At each point, we took a photograph of that point using a 14.2-megapixel Nikon D3100 DSLR camera equipped with an AF-S Nikkor 18-55 m lens (Nikon Corp, Tokyo, Japan). We used an ISO of 100, 1/250s shutter speed and automated F-stop. White balance was preset with a grey card using the camera's internal sensors prior to taking photos. To maximize the photo area, the camera was mounted at the top of a 3.5 m surveying pole and angled at 20° from nadir (Figure 2-7). At each ground truth point we placed a 1 m measuring stick on the ground and took a photo of point and its immediate surroundings. This processed created ~3x4 m photo that was later used as a highly-detailed reference image for each ground truth point (inset, Figure 2-7).

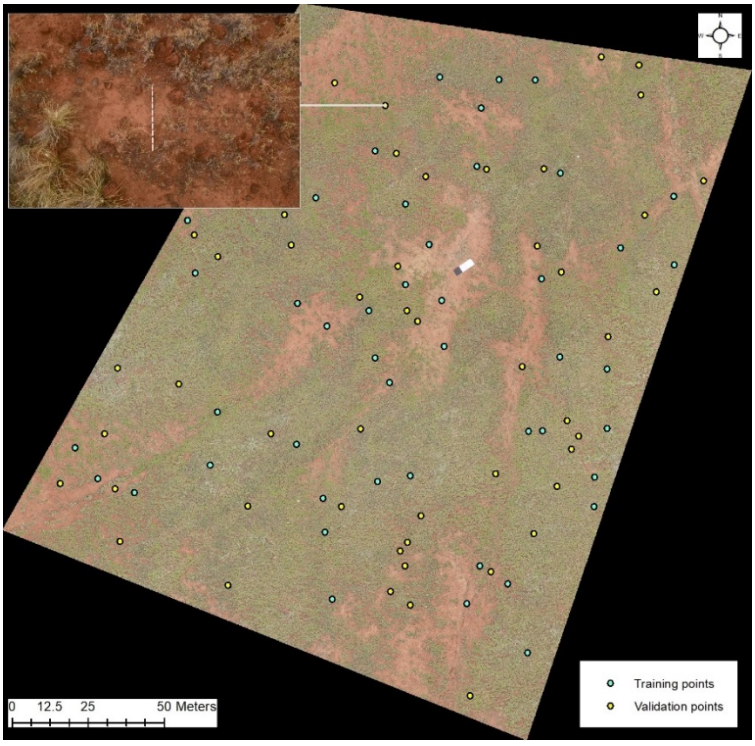

Figure 2-6: Locations of randomly-generated training and validation ground truth points. Inset photo shows example ground truth image.

Figure 2-7: Photograph of camera rig used to take ground truth images, with survey pole retracted to lowest height.

2.24 Image processing

Image processing involved a multi-step workflow (Figure 2-8). All data-collection mosaics were generated from raw imagery with Pix4D (Pix4D SA, Ecluben, Swizterland) image processing software, which has been successfully used in sUAS-derived mapping (Vallet et al. 2011, Turner et al. 2014, Lim et al. 2015). The software uses a feature-matching algorithm to identify tie points, which are then used to stitch together the images into a mosaic (Afek & Brand, 1998). To compare imagery created at the three different flight altitudes, we aligned the mosaics using our GCPs that were painted (prior to flights) on rocks within the study site. GCP data were incorporated into the mosaicking process using Pix4D by manually geotagging at least 10 images per GCP after the initial tie-point identification step.

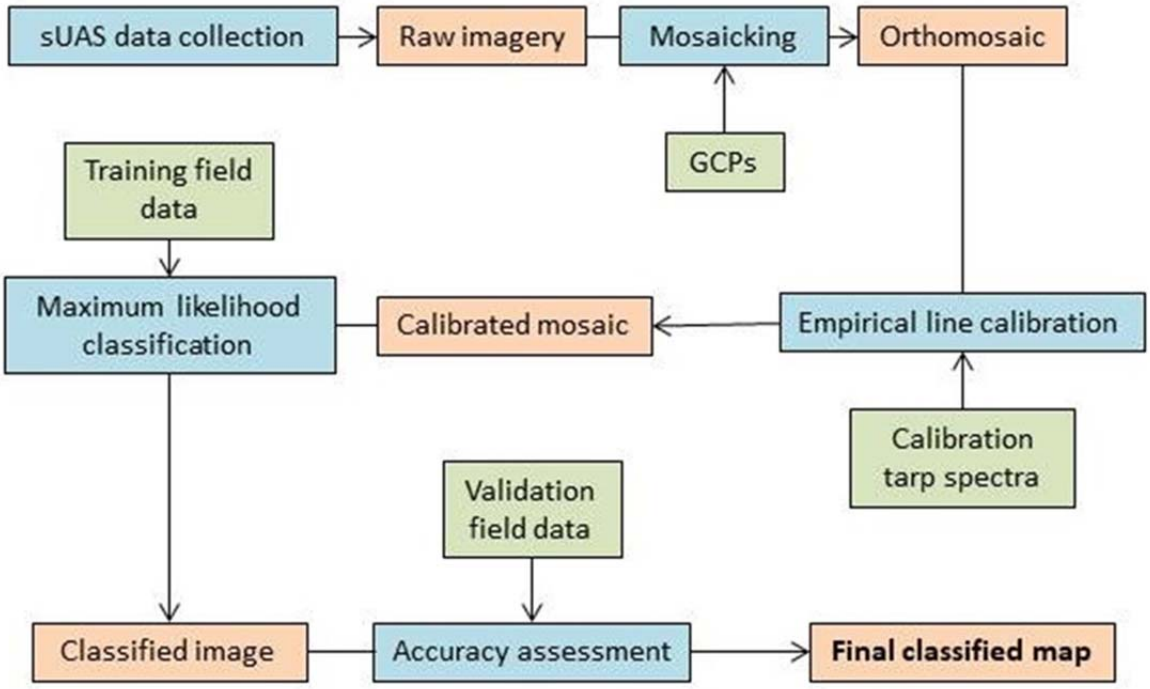

Figure 2-8: Flowchart of classification methodology. Processes are indicated by blue, outputs/inputs are in orange. Added data for specific processes is in green.

The resulting mosaics contained data in the form of digital number (DNs) for the red, green, and blue wavelengths in each pixel. A more useful unit of measurement for classification is reflectance, the ratio of reflected energy to incident energy on the surface (Teillet 1986), which allows for a quantitative assessment of pixel values at different wavelengths. One widely-accepted technique for calibrating imagery to reflectance is the empirical line method, which is based on the linear relationship between the reflectance and DN values of a surface (Baugh & Groeneveld 2008). This method converts DN values based on reference spectra with known reflectance values (Smith & Milton 1999). We chose to employ the empirical line method because of its ease of application for our data and its previous success with sUAS-derived imagery (Kelcey & Lucieer 2012, von Bueren et al. 2015, Wang & Myint 2015). We calibrated mosaics using ENVI v. 5.3 (Harris Geospatial Solutions, Boulder, CO) image analysis software. Our calibration targets were the 0.03 and 0.35 reflectance tarps present in each mosaic (we omitted the 0.56-reflectance tarp because it was overexposed in the imagery and thus did not provide reliable reference data).

We designated specific land cover classes (Table 2-2) and classified calibrated imagery in ENVI using the maximum likelihood algorithm.

Table 2-2: Descriptions of classes and subclasses used for image classification.

	Classes	Description
Major classes	Basal plant cover	All plant ground cover - shrubs, grasses and dry litter
	Bare ground	Exposed ground that is light brown-colored (does not contain visible surface biocrusts)
	Biocrust	All biocrust levels of development (1-3)
Biocrust subclasses	Biocrust LOD 1	Ground cover that is brown with small, scattered darker brown patches
	Biocrust LOD 2	Ground cover that is uniform dark brown or dark brown with patches of black
	Biocrust LOD 3	Ground cover that is uniform black or black with scattered patches of light brown (bare ground)

This algorithm incorporates probability when deciding the class assignment for each pixel by using calculated probability curves derived from training data for each class (Foody et al. 1992). The maximum likelihood algorithm compares the reflectance characteristics of each pixel and assigns pixels to classes based on the likelihood of a match to the reflectance characteristics of the training data (Chuvieco 2016). The algorithm assumes a normal distribution of reflectance values within each class and uses a Gaussian function to calculate probability:

$$p\left(\frac{x}{A}\right) = \frac{1}{\sqrt{2\pi\sigma_A^2}}\, exp\left\{-\frac{(DL_x - DL_A)^2}{2\sigma_A^2}\right\}$$

Equation 1: Function to determine the probability (p) of a pixel belonging to class A, where DL_A and σ_A are the mean reflectance values and the variance, respectively, of class A (Chuvieco 2016).

The advantage of this method is that it allows for overlapping spectral characteristics between classes, which aids in differentiation of classes that have similar spectra. We chose the maximum likelihood method because of its widespread use in remote sensing research and because of the spectral similarities between biocrusts and bare soil that we observed in our training data (Figure 2-9).

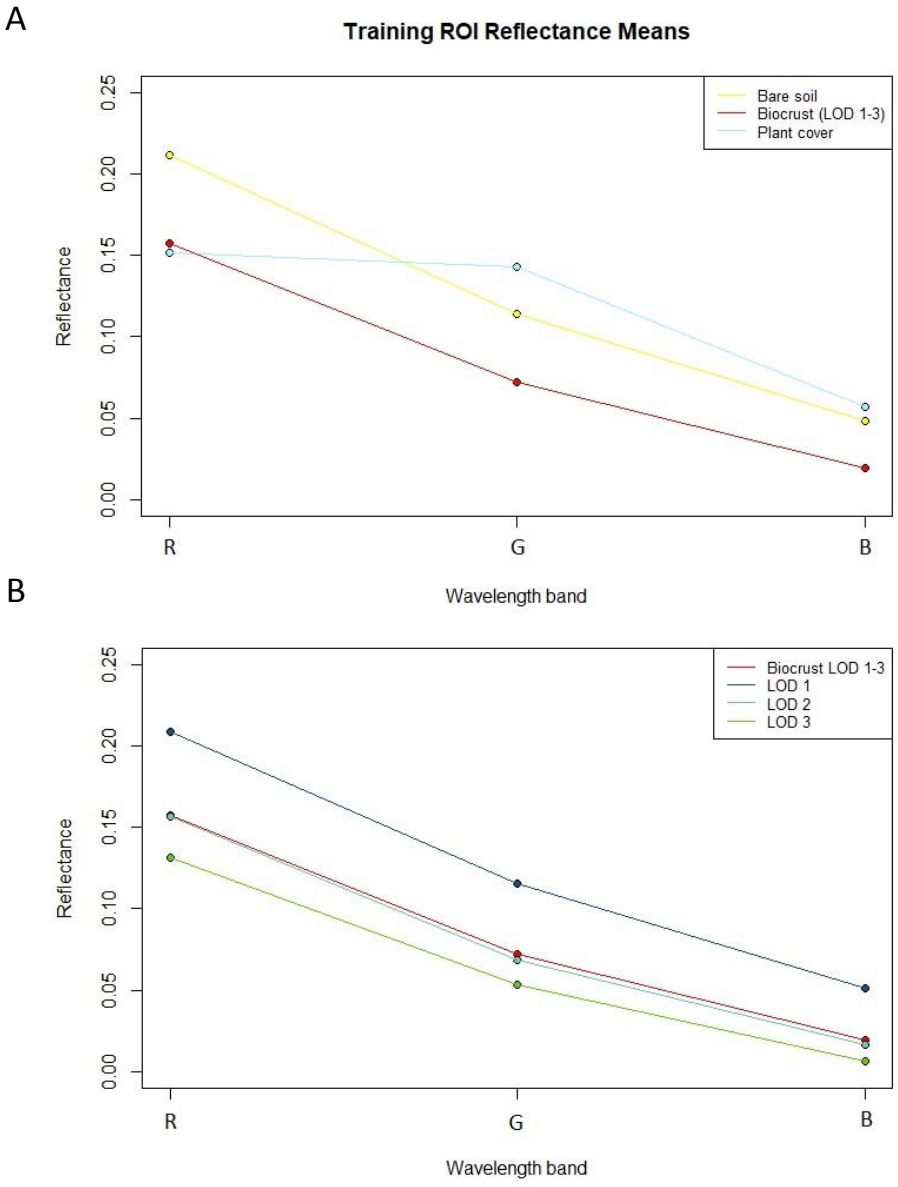

Figure 2-9: Charts of mean reflectance values derive from training data for (A) bare soil, biocrust (LOD 1-3) and plant cover, and (B) biocrusts at individual levels of development. Wavelengths R, G and B refer to the red, green, and blue bands, respectively.

Prior to classifying biocrust and bare soil, we conducted a preliminary classification using two classes: vegetation and non-vegetation. The plant cover class included living vascular plants as well as dry litter, which we generalized into one class because vegetation was not the focus of the project. After performing a post-classification accuracy assessment, we masked out the vegetation class and further classified the remaining non-vegetation pixels using two classes: bare ground and biocrust at any level of development (classification 1A). In addition, we created two more classifications: one with a bare soil class and a biocrust class that only encompassed higher levels of biocrusts development (classification 1B), which are more visually distinct from bare soil, and one with subclasses for individual levels of development (classification 2) (Figure 2-9B). Biocrust levels of development were defined using field observations coupled with definitions of biocrust morphological groups derived from the literature (Belnap et al. 2008). Since observations of biocrust development are somewhat subjective, we created a set of reference photos that were collected during preliminary fieldwork (Figure 2-11). This photo set allowed for judgements of biocrust development to remain consistent between mosaics. Rocks were very difficult to distinguish from soil or biocrusts and were therefore ignored in while creating both the training and validation data sets so that they would not influence accuracy assessments. Similarly, we did not classify shadows. Due to the sky conditions during data collection missions, no visually-distinct shadows were observed in the orthomosaics and there are no tall plants within the study area that would cast large shadows.

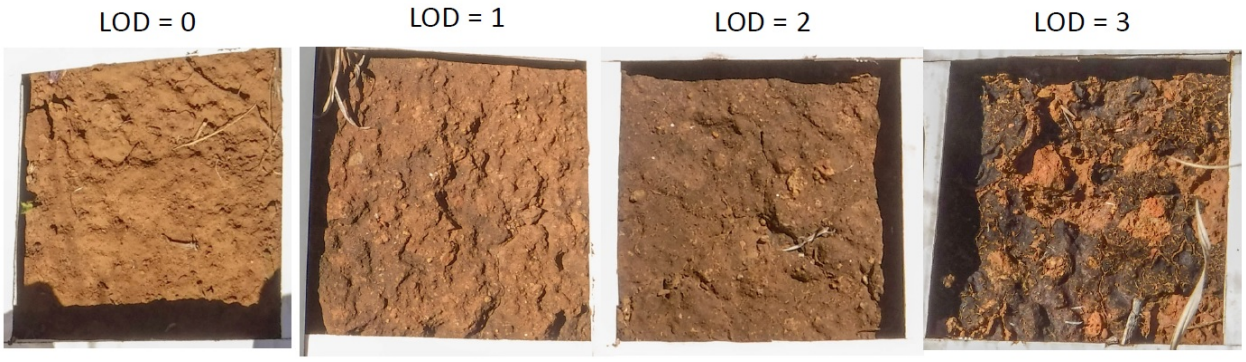

Figure 2-10: Representative images of each biocrust development level that was assigned its own class in classification 2.

To create training and validation data for imagery classification, we randomly divided our ground truth points (see section 2.14) into 2 groups with 50 points in each group. For both groups we manually drew the footprint of each ground truth photo over its corresponding point using the photos and the 40 m mosaic as guides for placement (Figure 2-11).

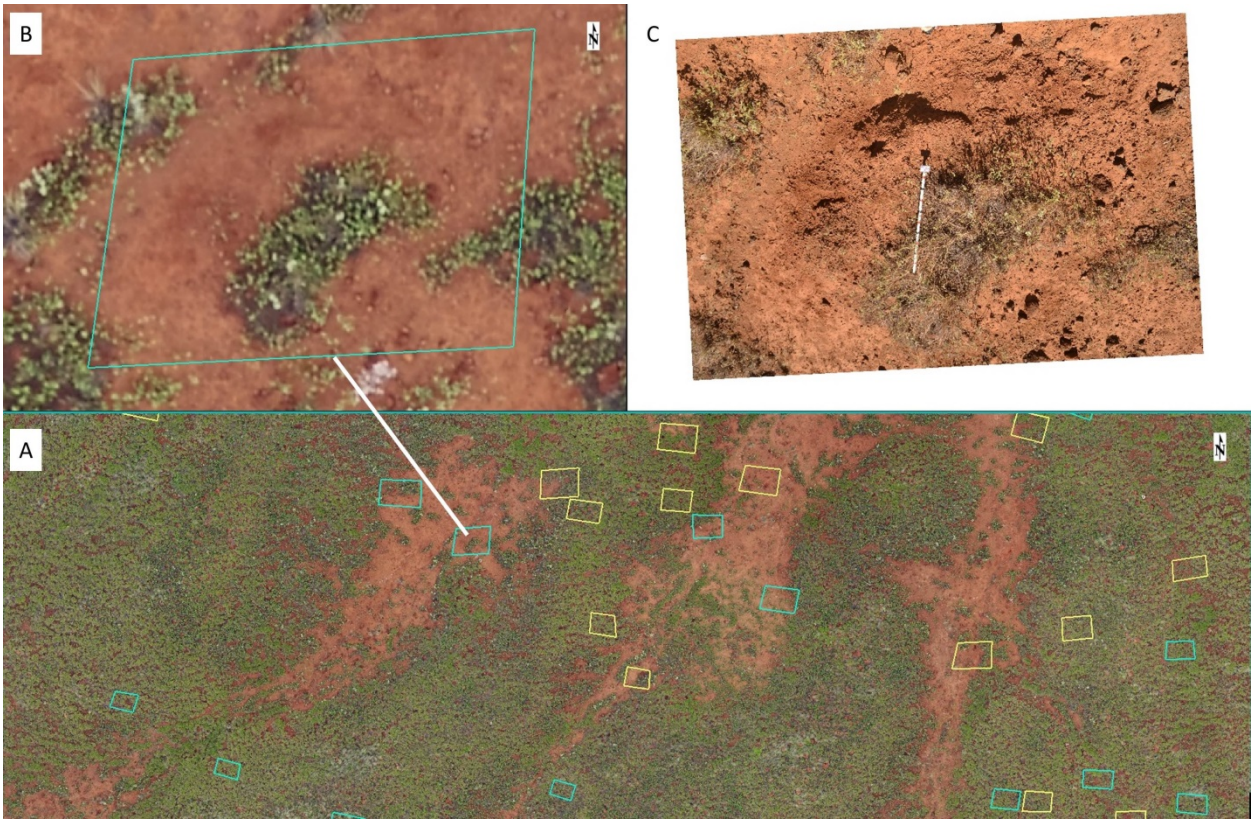

Figure 2-11: sUAS-derived mosaic at 1.15 cm/pixel showing larger extent (A) and zoomed-in (B) with corresponding ground truth photo (C). Cyan and yellow boxes indicate ground truth photo footprints for training and validation data sets, respectively. Length of measuring stick in ground truth photo is 1m.

We then created regions of interest (ROIs), groups of pixels assembled to create the training and validation data sets, by selecting pixels for each class on the 1.15 cm/pixel imagery based on information in the ground truth images. Finally, we classified each mosaic based on the training data, producing classified images at three different resolutions. ROIs were created separately for the training and validation points, generating two data sets: one for classifying and another for accuracy assessment.

After classifying the three orthomosaics, we performed accuracy assessments to compare the classifications conducted at different spatial resolutions. Using the validation data set, we generated a confusion matrix that compared class assignments created by the classification algorithm to the class assignments generated from field data. The matrix provided overall accuracy, the ratio of pixels that were correctly assigned to the total number of pixels in the validation data set, and a kappa coefficient, which is a metric of correct pixel assignment that factors in random chance. The confusion matrix also provided estimates of producer and user accuracies. Producer accuracy is related to the error of omission, which happens when a pixel should be classified into a particular class but is excluded (i.e., omitted). User accuracy is related to the error of commission, which is when the pixel is assigned to the wrong class. Together, these two metrics provide a more detailed understanding of the classification errors on a class-by-class basis.

2.3 Results

2.31 sUAS test flights

Adjusting exposure and using lens filters affected the reduction of bright spots in the mosaics (Figure 2-12). The imagery showed higher brightness on the left side than on the right side for the flight where exposure was automatic (flight 1EXP) and where exposure was auto-locked (flight 2EXP). Although there are no distinct bright spots, the brightness was still inconsistent across the mosaics. The addition of a polarized (P) filter (flight 1FLTR) or a ND8/P and a grid flight appeared to even out the brightness more, but variability was still visible in the upper left portion of the mosaic. A similar improvement was achieved with a line flight and the ND16/P filter (flight 3FLTR). However, bright spots remained visible regardless of the exposure settings and/or lenses used during the flights. The persistent occurrence of bright spots was validated through comparisons with soil color field observations. Soils in the study area were within the yellow-red hue category (YR), exhibited a narrow range of chroma values, and a wider range of saturation values (Table 2-3). Most of the soil was similar in color but comparisons with the test flight imagery revealed areas that were identified as the same color in the field yet had variable lightness in the mosaic (Figure 2-13).

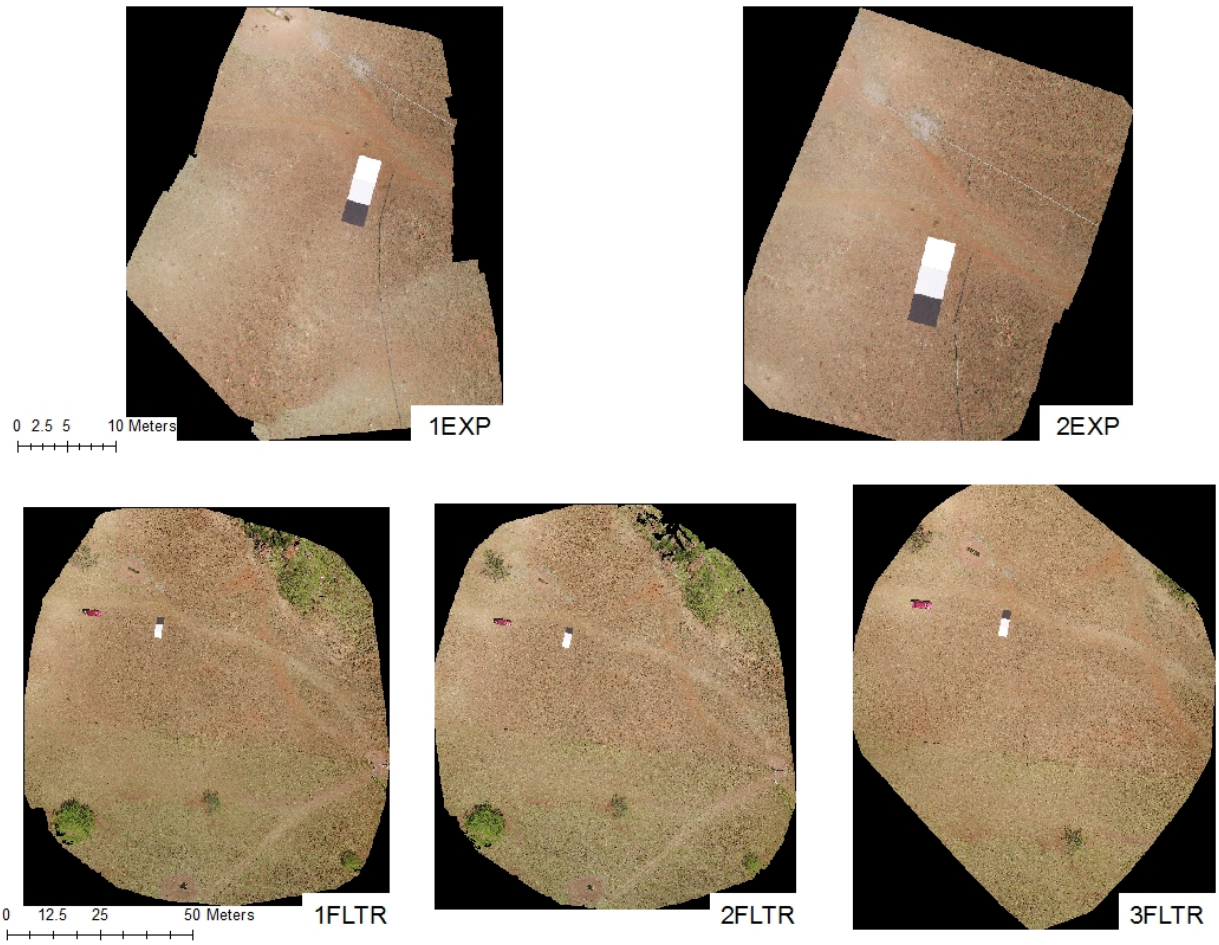

Figure 2-12: Mosaics generated from flights performed with exposure settings and lens filters described in Table 2-1. Labels indicate the flight used to generate each mosaic.

Table 2-3: Summary of Munsell colors recorded during soil color field data collection, with reference color chips obtained from a Munsell notation field guide (Munsell Color 1994).

Field data Munsell notation			
Hue	**Chroma**	**Saturation**	**Color chip**
2.5YR	5	1	
5YR	4	3	
7.5YR	3	2	
7.5YR	4	3	
7.5YR	4	4	
7.5YR	5	1	
10YR	3	2	
10YR	3	3	
10YR	3	4	
10YR	3	6	
10YR	4	2	

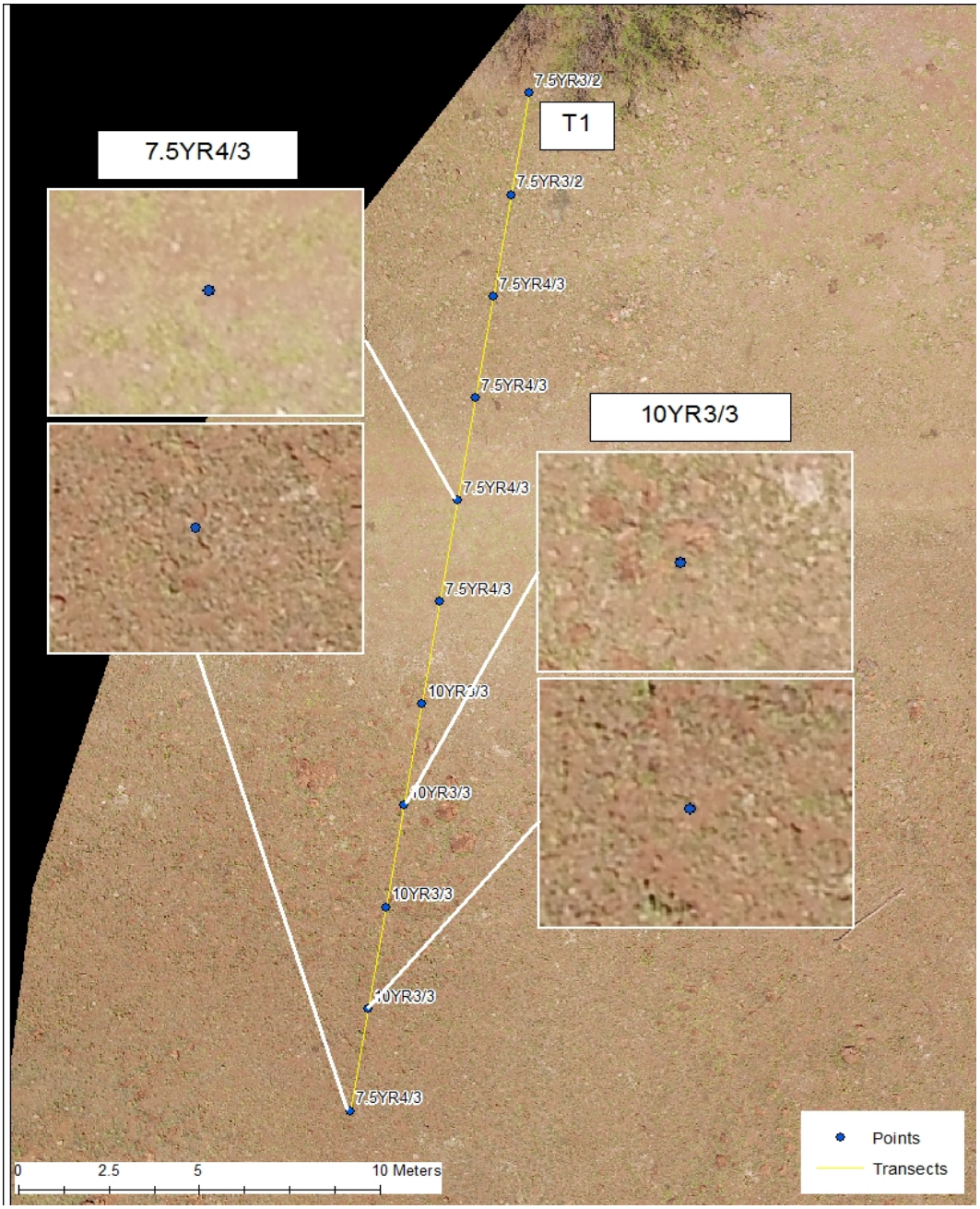

Figure 2-13: Mosaic generated from flight 3FLTR showing transect line 1 and corresponding soil color field data points. Point labels indicate Munsell color observed. Inset photos (zoomed-in on mosaic) show points where Munsell color was the same but the illumination intensity in the mosaic was different

2.32 Image classification

We created classified images showing land cover types at spatial resolutions of 1.15 cm/pixel, 2.05 cm/pixel, and 2.80 cm/pixel (Figures 2-14 and 2-16). Although it varied slightly among spatial resolutions, accuracy remained high (Table 2-4). The overall accuracy of the preliminary image classification (vegetation and non-vegetation) showed a downward trend as resolution decreased: 99.22% (kappa=0.9825) for the imagery collected at 1.15 cm/pixel, 96.35% (kappa=0.9248) at 2.05 cm/pixel and 96.07% (kappa=0.9186) at 2.80 cm/pixel. When the non-vegetation pixels were classified as either bare ground or any level of biocrust development, the overall accuracy decreased from 86.17% (kappa=0.7234) at 1.15 cm/pixel to 85.47% (kappa=0.6874) at 2.05 cm/pixel and then increased to 87.03% (kappa=0.7127) at 2.80 cm/pixel. However, the opposite trend was observed when the biocrust class included only those that were more highly-developed: accuracy increased from 86% (kappa=0.7198) at 1.05 cm/pixel to 87.27% (kappa=0.7460) at 2.05 cm/pixel, then decreased to 86.59% (kappa=0.7307) at 2.80 cm/pixel. The same trend was found when biocrust development levels were subdivided into individual classes (Figure 2-16). Overall accuracy increased from 53.64% (kappa=0.3799) at 1.15 cm/pixel to 60.24% (kappa=0.4686) at 2.05 cm/pixel and then decreased to 58.62% (kappa=0.4419) at 2.80 cm/pixel.

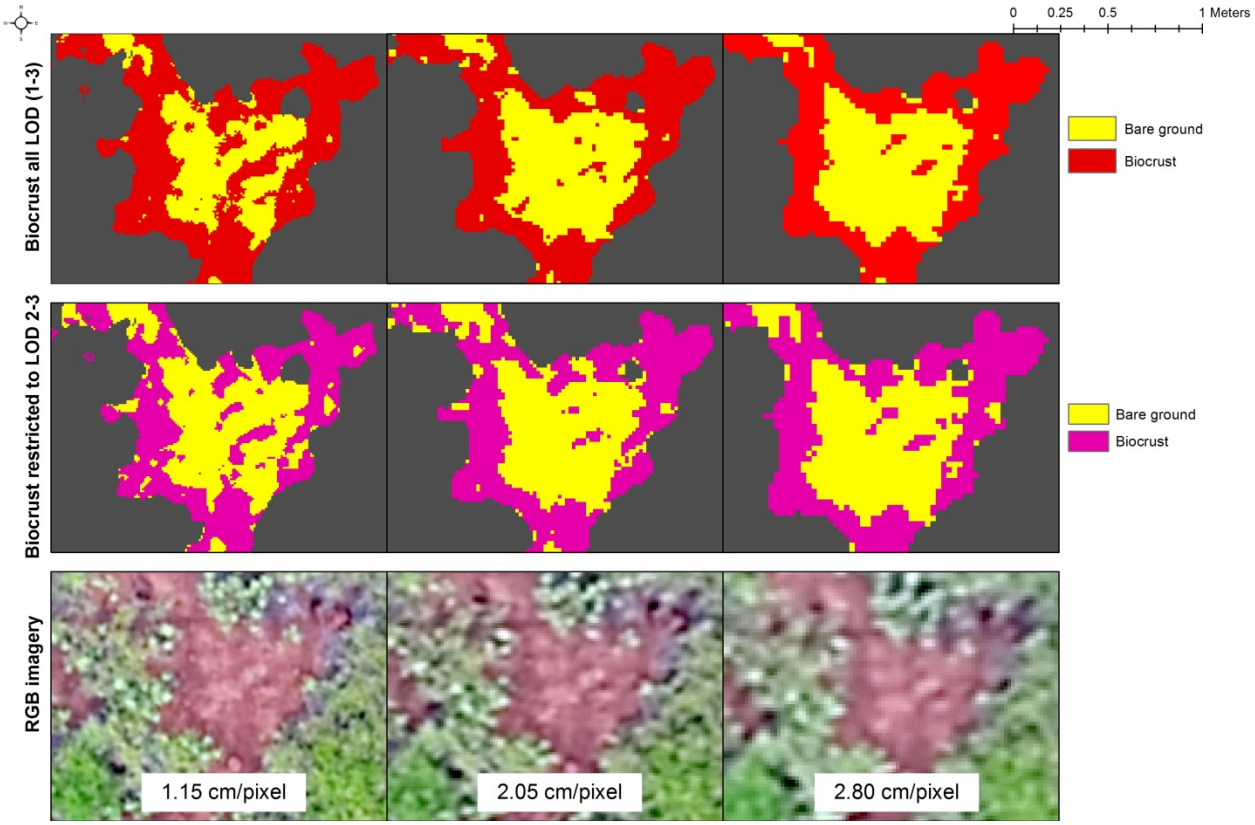

Figure 2-14: Subset of classified maps made with biocrust LOD 1-3 (top row) class and restricted to LOD 2-3 (center row) class at three different spatial resolutions. Vegetated areas are indicated by dark grey.

Table 2-4: Table of overall accuracy and kappa coefficients for different classification schemes at three different spatial resolutions. Preliminary classification included only vegetation and non-vegetation classes. Classification 1A included classes for vegetation, bare soil, and biocrusts (any level of development). Classification 1B included vegetation, bare soil, and all higher-order (>1) biocrust development levels. Classification 2 included vegetation, bare soil, and individual subclasses for each level of biocrust development (1-3).

	Preliminary classification		Classification 1A		Classification 1B		Classification 2	
Resolution (cm/pixel)	Overall Accuracy	Kappa Coefficient	Overall Accuracy	Kappa Coefficient	Overall Accuracy	Kappa Coefficient	Overall Accuracy	Kappa Coefficient
1.15	99.22%	0.9825	86.17%	0.7234	86.00%	0.7198	53.64%	0.3799
2.05	96.35%	0.9248	85.47%	0.6874	87.27%	0.7460	60.24%	0.4686
2.80	96.07%	0.9186	87.03%	0.7127	86.59%	0.7307	58.62%	0.4419

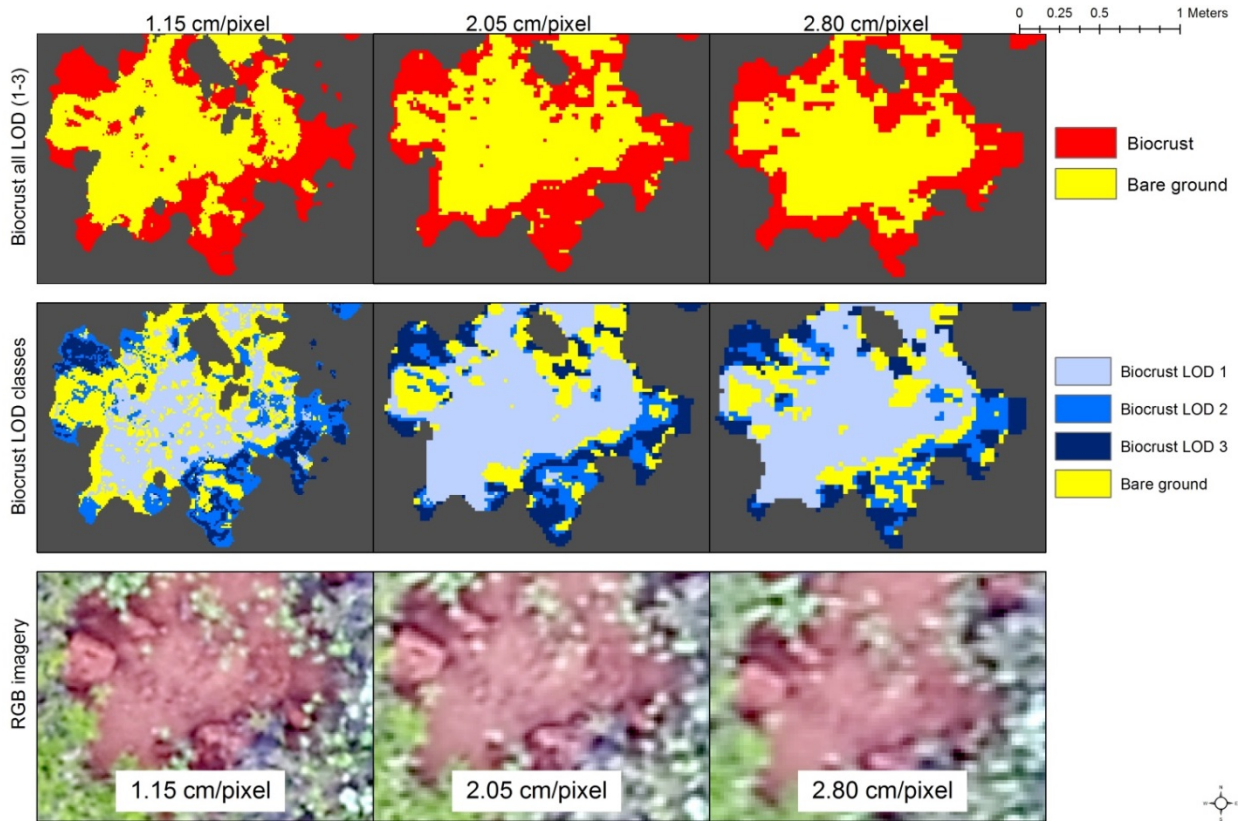

Figure 2-15: Subset of classified maps made with a single biocrust LOD 1-3 (top row) class and individual LOD subclasses (center row) class at three different spatial resolutions. Bottom row shows imagery used for classification training and validation.

Producer accuracy, a measure of omission errors, varied among the classes and spatial resolutions with no consistent relationship between producer accuracy and resolution (Figure 2-16). Producer accuracy was generally highest for the plant cover class and lowest for the biocrust class at all resolutions, regardless of whether the biocrust class was restricted to higher levels of development. However, the producer accuracies for biocrusts in classification 1A (biocrust LOD 1-3) were higher than classification 1B (biocrust LOD 2-3) at the 2.05 cm and 2.80 cm pixel sizes and slightly lower at the 1.15 cm pixel size.

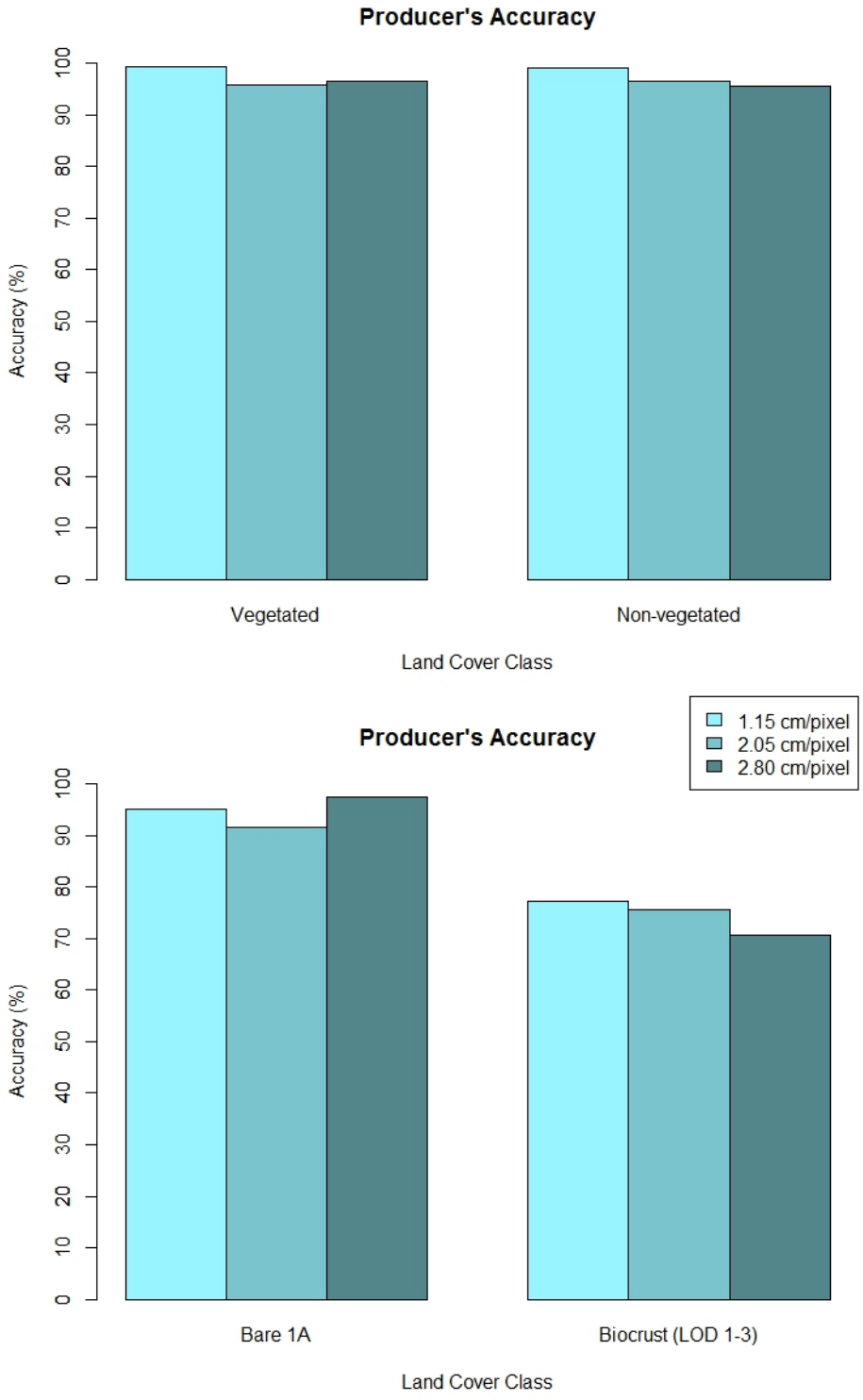

Figure 2-16(A): Producer accuracies at three spatial resolutions for preliminary classification (top) and classification 1A (bottom). Progressively darker shades of blue represent increasingly coarse spatial resolutions.

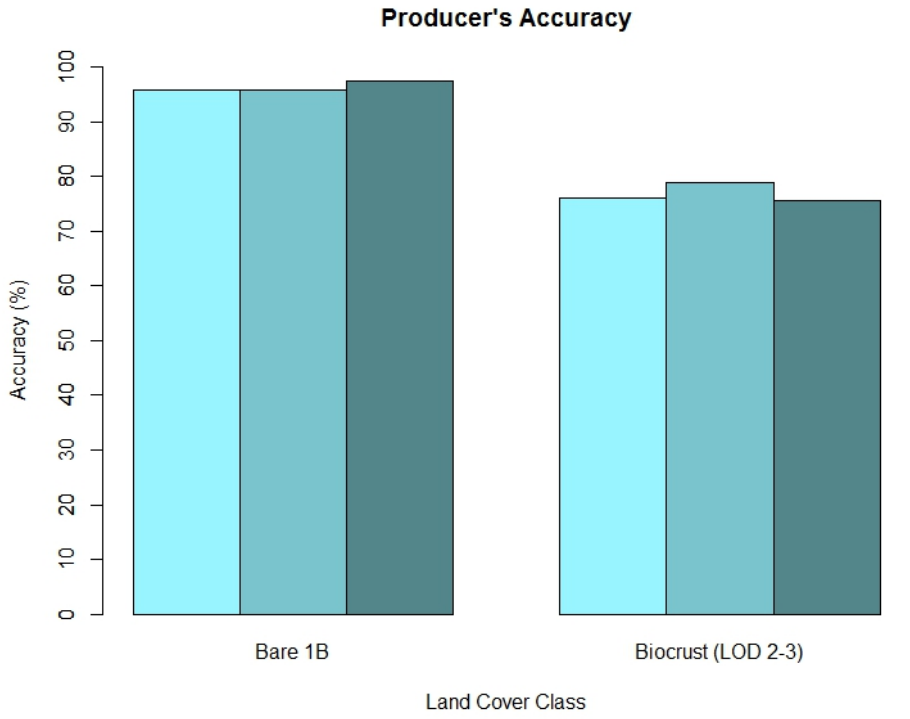

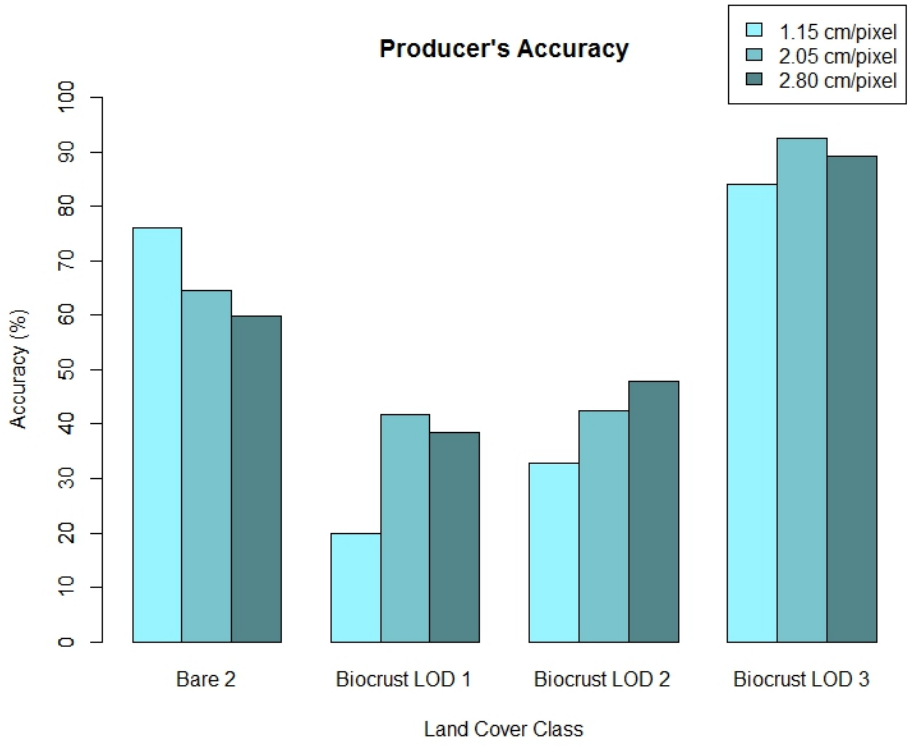

Figure 2-16(B): Producer accuracies at three spatial resolutions for classifications 1B (top) and 2 (bottom). Progressively darker shades of blue represent increasingly coarse spatial resolutions.

The producer accuracies for individual levels of biocrust development were much lower than for other land cover classes, although accuracy generally increased as development level increased (Figure 2-16B, lower panel). Among the different spatial resolutions, producer accuracy was highest for biocrust LOD 2 and 3 at 2.80 cm/pixel, and for LOD 1 at 2.05 cm/pixel. Within the levels of development, the producer accuracy either increased as resolution increased (LOD 2), or increased as resolution increased from 1.15 to 2.05 cm/pixel and then decreased as resolution increased from 2.05 to 2.80 cm/pixel (LOD 1, and to a lesser extent, LOD 3).

User accuracy, a measure of commission errors, varied between land cover classes and spatial resolutions, with no consistent relationship between spatial resolution and user accuracy (Figure 2-18). User accuracies were equal or higher for biocrusts in classification 1A than in classification 1B at all three resolutions. Biocrusts in classification 1A had a pattern of decreasing and then increasing accuracy as pixel size increased, while biocrusts in classification 1B showed a slight increase in user accuracy as pixel size increased. Among individual biocrust levels of development, user accuracy was higher than producer accuracy in some classifications but not in others. Within individual LOD classes, there was also no clear relationship between user accuracy and spatial resolution.

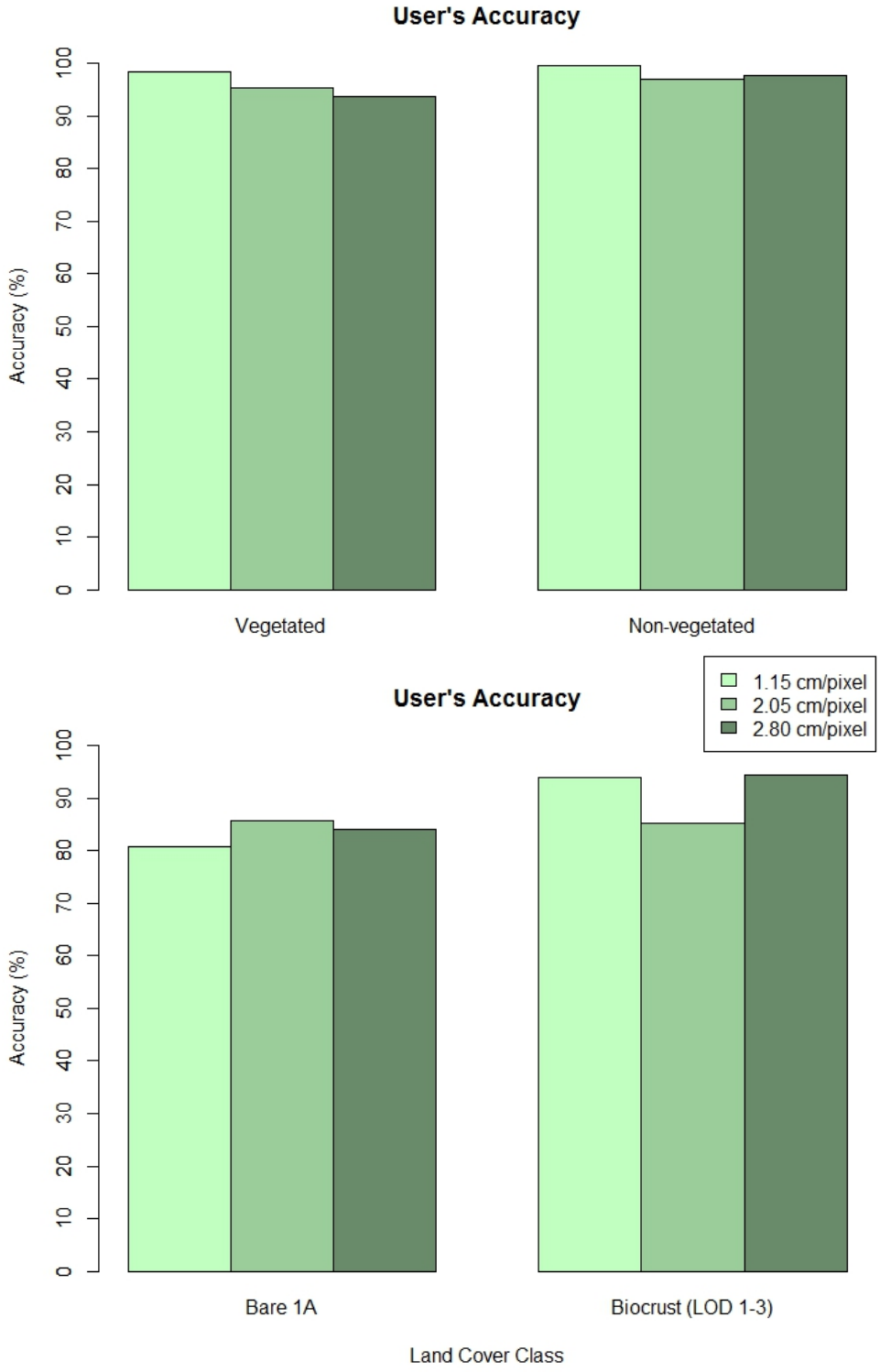

Figure 2-17(A): User accuracies at three spatial resolutions for preliminary classification (top) and classification 1A (bottom). Progressively darker shades of green represent increasingly coarse spatial resolutions.

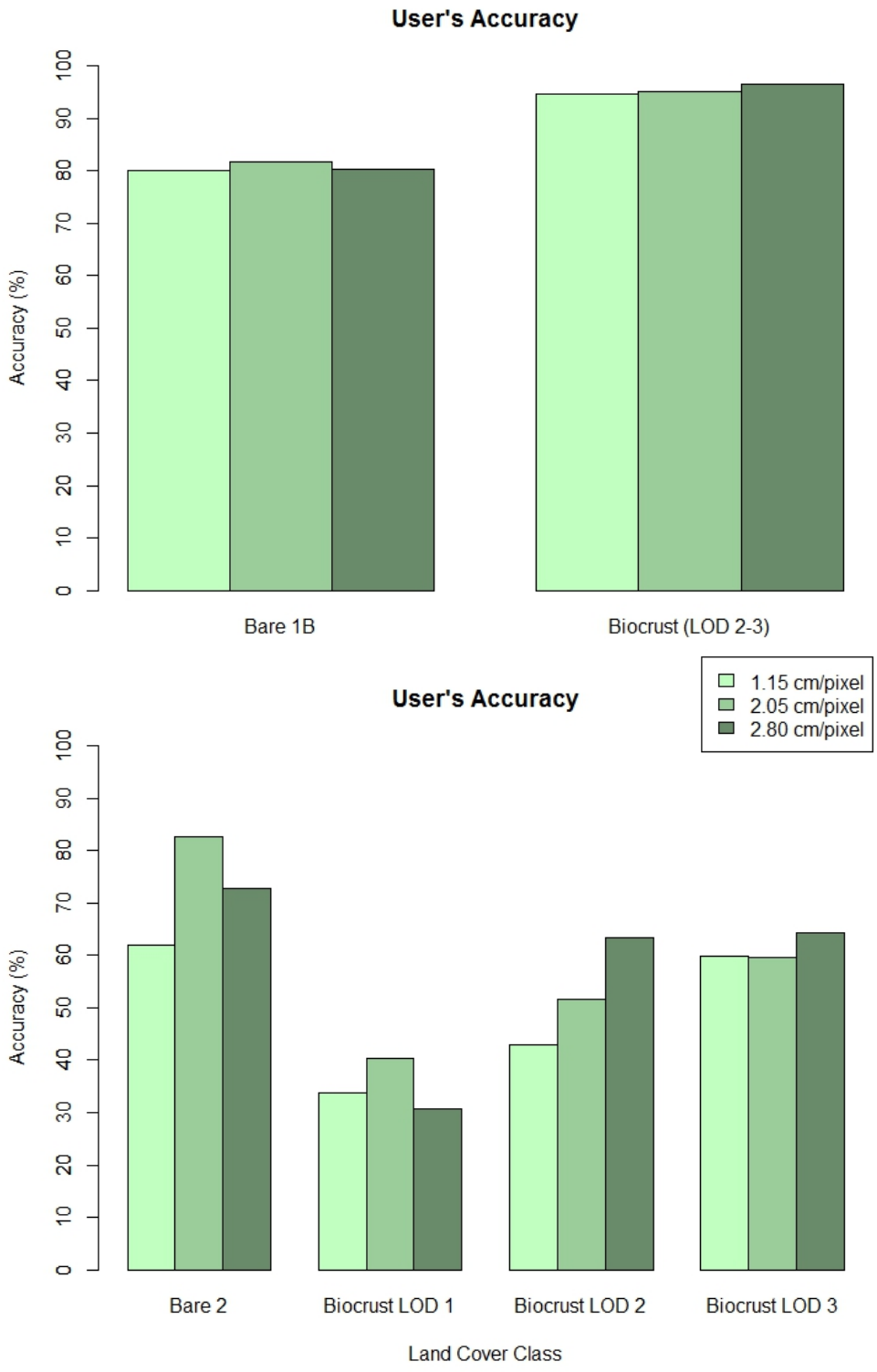

Figure 2-17(B): User accuracies at three spatial resolutions for classifications 1B (top) and 2 (bottom). Progressively darker shades of green represent increasingly coarse spatial resolutions.

2.4 Discussion

2.41 sUAS test flights

Although these flights were initial experiments with an emerging technology, they provided useful information on the effects of exposure settings and lens filter on imagery collected under clear, sunny skies at our field site. We found that both exposure settings produced similar results on brightness across each mosaic. We also found that the combination of a ND16/P filter and a line flight pattern produced comparable results to a P or ND8/P filter and a grid flight pattern. We did not test the combination of ND8/P or P filters and a line flight pattern, or a ND16/P filter and a line flight, so we cannot say whether the lens filter or the flight pattern was the most important parameter for evening out brightness across a mosaic. Further research with more combinations of lens filters and flight patterns would shed light on which is the most important contributor to bright spot reduction. A more standardized investigative approach would also provide further insight into methods to minimize bright spots. However, our results indicate that solar artefacts can persist even in the presence of high image overlap and lens filters. Therefore, we decided to collect subsequent aerial data under overcast skies or when the sun was otherwise obscured, such as immediately after dawn before the sun rose above nearby mountain peaks. We flew without lens filters because they were unnecessary under these sky conditions and used a line flight pattern to conserve battery and maximize coverage.

2.42 Image classification

When biocrusts were grouped together into a single class (classifications 1A and 1B) the overall accuracies show that the sUAS-derived method generated accurate classified maps for distinguishing between biocrusts and bare ground at all three spatial resolutions. However, the relationship between accuracy and spatial resolution was not what we expected. We hypothesized that accuracy would decrease as resolution decreased but we found that to be the case only in specific situations, such as the producer accuracy for biocrusts in classification 1A. The reasons for the variations in accuracies that we observed are unclear, but there are a few possible explanations. One potential reason is the pixel size changes that occur as resolution decreases. As pixels get larger, the data they contain becomes generalized over a larger area. When a very high-reflectance pixel and a very low-reflectance pixel get merged together into one

larger pixel, the mean reflectance in the larger pixel will dictate which the class assignment of that pixel. Therefore, an area that may appear as the boundary between biocrusts and bare soil at higher resolutions may get shifted into either complete biocrust or bare soil at lower resolutions.

Another possible reason is the inherent function of the classification algorithm. Upon visually inspecting the results of each classification, we observed differences in pixel assignments among different resolutions. For example, in Figure 2-15 the center portion of the biocrust/bare ground patch shows distinct sections of biocrust at the 1.15-cm pixel size (top row, left image) that seem to disappear at lower resolutions (top row, middle and right images). An exploration of the rule images – raster visualizations that quantify the extent to which each pixel matches each class – revealed that for some pixels the difference between the strength of the match to the biocrusts class vs. the bare ground class was very small. The maximum likelihood algorithm classifies pixel according to the highest probability of a match, but if the probabilities are nearly the same then a pixel may get assigned differently based on minute differences among the mosaics. This amplification of small differences would subsequently affect the accuracy among different images.

In addition, variations in accuracies may be due to the masking process. Since masking was conducted on each mosaic separately, each masked image contained slightly different pixels available for classification. In addition, each mask was based on a classification, so the afore-mentioned potential class assignment differences would affect the mask itself. Therefore, a comparison between classified images would show differences simply due to the pixels present, which is evident by the differing edges among the classified patches shown in Figure 2-15. These differences could also influence accuracy rates by presenting pixels in some classified images that are not present in others.

Regardless of the underlying reasons, the variations in overall accuracy among images at different spatial resolutions were very small – less than 3.5%, with the exception of classification 2 (which showed accuracy differences of less than 7%). Exploratory comparisons of different spatial resolutions using a pairwise t-test showed no statistically-significant difference ($p>0.05$) in overall accuracies or kappa coefficients between 2.05 cm/pixel and 2.80 cm/pixel maps or between 1.15 cm/pixel and 2.05 cm/pixel maps. Therefore, any detrimental impacts of classifying at the coarser resolution would be negligible. Our findings show that accuracy

decreases only slightly as spatial resolution increases, indicating that data collection missions can be flown higher without significant compromises on classification.

Despite high overall accuracies, the accuracy of the classification scheme differed among the various land cover classes. Predictably, the most accurately-identified were the vegetated and non-vegetated classes in the preliminary classification, which had low omission and commission errors across all spatial resolutions (Figure 2-17). This ease of classification comes from the spectral patterns of vegetation (and dry litter) in the visible wavelengths, which differ from those of exposed soil more than the spectral patterns of bare soil differ from those of the biocrusts at this particular study site (Figure 2-8). Differentiating between bare soil and biocrust was more difficult due to the spectral overlap of these classes within the visible range, which has also been observed in other studies (Rodriguez-Caballero et al. 2017). When we restricted the biocrust class to the more readily-visible levels of development (2 and 3 only) we found that both user and producer accuracies were equal to or greater than the accuracies for the all-encompassing biocrust class (LOD 1-3). The generally higher accuracy of the more restricted biocrust class further implies that the classification algorithm has trouble differentiating between bare soil and biocrusts, but shows that the classes can be refined to improve classification accuracy while still identifying the majority of surface biocrusts.

The accuracy of the classification dropped substantially across all spatial resolutions when the biocrust class was subdivided into the varying levels of development, which had significantly lower individual class accuracies. Individual levels of development were defined according to their visual appearance and progressively-darkened surface, which created classes with extensive spectral overlap. The maximum likelihood algorithm was able to distinguish between biocrust and no biocrust, but was not sensitive enough to reliably separate different levels of biocrust darkness (i.e., different LOD). Considering that all the biocrust found at the study site exhibited the same color gradient, it is likely that all of the biocrust at this site were of the same type – most likely cyanobacteria-dominated based on comparisons found in the literature (reviewed in Belnap et al. 2018). The homogeneity of the biocrust cover makes differentiating between development levels using only visible light wavelengths especially difficult. However, other areas with more varied biocrust characteristics or greater differences

between biocrusts and their surrounding soil (for example, dark biocrusts against desert sands) may be able to apply this method and parse out development levels more accurately.

In addition, the use of sensors with greater spectral capabilities could improve the accuracy of identifying levels of development. Lab-based spectral analysis of biocrusts have given rise to various spectral indices that could be used for mapping (Karnieli et al. 1997, Chen et al. 2005) but the results from early exploratory analyses conducted for this project indicated that these indices would not be reliable tools for classification from our sUAS imagery. These methods were not usable for this project because of the limited spectral resolution of our sensor and the types of biocrust present at the study site, but at other sites with greater biocrust diversity these tools may be useful for identifying different stages of biocrust development. There are, however, other approaches that could improve the accuracy of biocrust classifications performed with our method. Biocrusts have been found to have different spectral properties based on their moisture level and in particular show lower reflectance after wetting (Karnieli et al. 2001, Rodriguez-Caballero et al. 2015, Rozenstein & Adamowski 2017). Collecting data immediately after rainfall events may allow for better differentiation between wet biocrusts and bare soil, although the wetting effects on soil reflectance would also need to be considered. Also, our method relies on measurements of reflectance, but it is possible that biocrusts could be identified using another method for measuring pixel values, such as Munsell colors, which have been used in previous studies to describe biocrust characteristics (Graef et al. 2000, Grishkan et al. 2013). It must be noted, however, that converting raw DNs to Munsell color notation would likely require a color calibration surface, similar to the reflectance tarp in our imagery, so that colors could be standardized and compared between mosaics.

The relationship between the producer and user accuracies for the bare soil and biocrust classes provides insight into mapping biocrusts and bare soil relative to each other. The producer accuracy was generally lower than the user accuracy for biocrusts, which indicates a higher chance of omitting biocrusts in places where they occur (error of omission) than of including biocrusts in locations where they do not actually occur (error of commission). The implication of this error pattern is that this classification scheme underestimates biocrust coverage. Conversely, the bare soil class had higher user accuracies than producer accuracies, indicating that the bare soil is more likely to be classified as such in areas where it does not actually occur than omitted

from areas that it does actually occur. This leads to an overestimation of bare soil coverage. The implication of this combination of errors is that this method provides biocrust classification that can be a useful, conservative estimate in land cover studies.

If we consider the ratio between our spatial resolution values, we see that our lowest resolution (2.08cm/pixel) corresponds to an approximately 1.8 times larger pixel size than our highest resolution (1.15cm/pixel). This 1.8X increase in pixel size translates, on average, to a 4.9% change in producer accuracy and a 5.8% change in user accuracy. This is comparable to classifications produced from satellite-based LANDSAT 30m pixel-size imagery, which have shown an average 6.1% change in accuracy across a 2X ratio of spatial resolutions (Latty & Hoffer 1981). Our results are higher-accuracy than some previous studies relating flight altitude and classification accuracy using the same ratio of resolutions (Pena et al. 2015) but comparable to the results of others (Torres-Sanchez et al. 2014), indicating that there are also situation-specific factors that influence classification accuracy.

Previous remote sensing classifications of biocrusts have produced a range of accuracies, from kappa coefficients of 0.6 (Rodriguez-Caballero et al. 2017) to a 94% overall accuracy and a 0.92 kappa coefficient (Rodriguez-Caballero et al. 2014). The higher accuracies in this range were obtained from hyperspectral data whereas our results were obtained from RGB imagery, demonstrating that accurate biocrust mapping can be performed with relatively simple equipment. Furthermore, previous classifications were performed on imagery at a spatial resolution of 1 m (Rodriguez-Caballero et al. 2014, 2017), which is much lower than the resolutions that we obtained with the sUAS platform. Biocrust distribution can vary across very small distances, so it is advantageous to map them with as much detail as possible. Our results show that very high-resolution imagery can be combined with pixel-based classification schemes to produce accurate maps that show biocrust distribution at small spatial scales and with high detail.

Although research on biocrust classification from sUAS-derived imagery is lacking, our results can be compared to similar studies that use the sUAS platform to create land cover classifications. Our results provided higher accuracy than pixel-based classifications of seabed cover (Ventura et al. 2016) and comparable accuracy to classification of mussel beds (Gomes 2018), which were both in marine ecosystems but share our challenge of classes with similar

spectral characteristics (fine and coarse sand for Ventura et al. 2016 and mussels and black rocks, in the case of Gomes et al. 2018). Compared to a sUAS-derived classification conducted in a rangeland ecosystem, our overall accuracies are similar to object-based classifications that included dark and light non-vegetated areas – such as those with and without biocrusts (Laliberte et al. 2011). Some researchers have argued that that object-based classification approaches are more reliable than pixel-based methods (Yu et al. 2006), but our results indicate that pixel-based classification remains a reliable tool for biocrust mapping at small spatial extents.

Although landscape metrics are influenced by spatial scale (Turner et al 1989), the effects of pixel size on landscape metrics are reduced for classification schemes with overall accuracy approaching 90% (Shao & Wu 2008). Our methodology involves a commercially-available, relatively inexpensive platform mounted with a sensor that requires no special calibration prior to imagery collection. This setup opens the doors for further research by providing a way to map biocrusts at fine spatial resolutions and small spatial scales using equipment that is accessible for researchers and conservation managers. Our method can be readily applied to a variety of spatial ecology research questions. Biocrusts play important roles in a multitude of ecosystem processes: nitrogen cycling (Delgado-Baquerizo et al. 2013), soil hydrology (Zhao et al. 2013, Bowker et al. 2013), soil function (Antoninka et al. 2016), and responses to climate change (Maestre et al. 2013). Knowledge of highly-detailed spatial distribution of biocrusts could be used to further investigate these roles in relation to other landscape characteristics and processes that can vary over small spatial scales such as microtopography, parent material, or wildfires. In the next chapter we will discuss our application of very-high resolution classified images to investigate the role of biocrusts on the landscape processes of soil transport and erosion in the Kawaihae watershed.

Chapter 3: Biocrusts, soil loss, and grazing animals

3.1 Introduction

Using the image classification method described in Chapter 2 and based on discussions with Kawaihae watershed land managers, we identified three key research questions related to the role of biocrusts in erosion mitigation. First, we wanted to understand the relationship between soil stability and biocrust development in this watershed because the landscape of the Kawaihae watershed is considered at high risk for erosion (Stewart 2005, Oceanit Center 2007). Although biocrusts have been found to directly contribute to soil surface stability (Chaudhary et al. 2009), their composition and effects on soil stability may vary between locations (Belnap et al. 2018). We hypothesized that soil stability would increase with biocrust development level, based on previous research that found a positive, linear relationship between development and soil stability class for biocrusts that are morphologically similar to those found at our study site (Belnap et al. 2008). To answer this question, we collected soil aggregate stability field data, which has been shown to be associated with susceptibility to erosion (Barthes & Roose 2002), and compared it against classifications of biocrust development levels.

Our second research question addressed soil loss in the presence of biocrusts. The Kawaihae watershed has been the subject of previous research that quantified relative erosion risk across the landscape (Oceanit Center 2007). However, the spatial data used in that study were much lower-resolution that what was available to us and did not consider biocrusts as a land cover class. In addition, the use of lower resolution data precluded the reliable application of those results to conservation initiatives, such as the placement of check dams, which are much shorter than the typical pixel size of the imagery used in the previous research. We sought to estimate the fine-scale spatial distribution patterns of soil loss and to quantify its severity over time, and then compare those characteristics with biocrust distribution to more fully understand the direct impact of biocrusts on erosion. We hypothesized that areas with biocrust present will have less soil loss over time than areas without biocrust because of the known positive relationship between biocrust cover and soil stability. To answer this question, we used our classified imagery in conjunction with previous sUAS imagery collected at the same site 33 months (2.75 years) prior to our study. Using orthomosaicas and Digital Surface Models (DSMs)

derived from these two data sets we compared the spatial dimensions of soil loss across the intervening time span.

Our final research question addressed the influence of grazing animals on biocrust abundance in the watershed, because the land is currently grazed by cattle and feral ungulates. To understand the influence of these disturbance factors, we compared grazed and non-grazed sites using a space-for-time substitution approach that utilized a previously-fenced grazing exclosure area directly adjacent to a grazing-accessible area. Because cyanobacteria biocrusts are sensitive to chronic disturbances such as trampling (Kuske et al. 2012), we hypothesized that biocrust abundance (as determined by area of coverage) would be lower at the site where grazing animals are present than at the site where they are excluded. We used our previously developed classification methodology (see section 2.2) to generate classified maps of biocrusts and other land cover types and compared the area of coverage of each land cover in the grazed and exclusion sites.

3.2 Methods

3.21 Study site

The study area for these research questions was located in the same section of the watershed where we conducted previous biocrust research and therefore had the same elevation, climate, rainfall and vegetation composition (see section 2.21). As in our previous research (see Chapter 2), this site was chosen because of its designation as high-risk for erosion (Oceanit Center 2007) and because we had access to previously-collected aerial data at that location. The soil type across the study area is Kawaihae series with a 12-20% slope (Natural Resource Conservation Service 2013), which is characterized by very cobbly, fine sandy loam with a loose structure (Sato et al. 1973), overlaying `a`a lava bedrock (NRCS 2013). The soil has moderate permeability and water holding capacity (NRCS 2013).

The study sites are contained within a larger paddock and are all located within 500m of each other (Figure 3-1). A cattle herd of approximately 461 animals owned by the Parker Ranch of Waimea is rotationally grazed across 14 paddocks in the Kawaihae watershed year-round (Gordon Kalaniopio, Parker Ranch staff, personal correspondence). There is no pre-determined schedule for rotation between paddocks, but the herd spends an estimated 3-4 days at a time

crossing the 566.2-acre paddock that contains the study site. Approximately 300 feral goats (Gordon Kalaniopio, personal correspondence) are also present in the watershed and have been observed regularly within the paddock encompassing the study site. We were unable to determine the precise date of exclusion fence construction, but we determined from conversations with Parker Ranch and Kohala Watershed Partnership staff that the exclusion site has been fenced for at least 10 years (Gordon Kalaniopio, personal correspondence; Cody Dwight, personal correspondence).

Figure 3-1: Map of Kawaihae watershed with grazing exclusion and soil loss (erosion) research sites in yellow. Inset map shows location of watershed on Hawai`i Island.

3.22 Field data collection

Biocrust field samples were collected in August-December, 2018, using a non-random approach so that varying levels of development would be equally represented. Samples were collected (n=60) at least 3 m apart and separated by vegetation, rocks, or dry litter to ensure independence of samples. Each biocrust sample was categorized as loose, non-crusted soil or biocrust LOD 0-3 (n=12 per category) using previously-established visual criteria (see section 2.22); field-observed LOD was recorded and a picture of the sample was taken using a 16 Megapixel Nikon CoolPix point-and-shoot digital camera (Nikon Corporation, Tokyo, Japan) and a calibration grey card for later verification. Six subsamples (6-8 mm in diameter) were collected from across a 6x6 cm quadrat placed over the center of each biocrust patch.

Soil stability was testing using a field soil aggregate stability kit (Figure 3-2) (Herrick at el. 2001). The kit contains 18 sieves that are open on one end and have 1.5-mm mesh covering the opening on the other end. These sieves fit into the sample sections of the boxes (Figure 3-2). The kit is accompanied by a soil stability class table (Table 3-1A) which describes the soil stability classes (Herrick at el. 2001).

Figure 3-2: Photograph of soil stability kit with biocrust samples. Inset photo is a close-up of a single sample with size estimation grid visible underneath.

Table 3-1: Description of the criteria used to establish soil stability classes after initial testing (A) and with extended classes (B).

	Stability Class	Description
A		
	1	50% of structural integrity lost (melts) within 5 seconds of immersion in water AND < 10% remains after 5 wet sieving cycles, OR soil too unstable to sample (falls
	2	50% of structural integrity lost within 5-30 seconds of immersion AND < 10% remains after 5 wet sieving cycles
	3	50% of strucural integrity lost within 30-300 seconds (5 minutes) of immersion AND < 10% remains after 5 wet sieving cycles
	4	10-25% of sample reamins after 5 wet sieving cycles
	5	25-75% of sample remains after 5 wet sieving cycles
	6	75-100% of sample remains after 5 wet sieving cycles
B		
	6	< 10% of original sample remains after 10 seconds of shaking
	7	10-25% of original sample remains after 10 seconds of shaking
	8	25-75% of original sample remains after 10 seconds of shaking
	9	> 75% of original sample remains after 10 seconds of shaking

To perform soil aggregate stability testing, the wells of the box were filled 2/3 to the top with distilled water. Each sample was placed in a well as shown in Figure 3-2 and immersed for 5 minutes. Samples were then wet sieved by immersing and lifting the sieve containing the samples every 2 seconds, for 5 lift-immerse cycles. After wet sieving, all samples were examined and categorized into stability classes (Herrick et al. 2001). Per field kit recommendations, all soils were sieved regardless of stability class. To ensure consistent measurements of the proportion of original sample remaining after sieving, we employed a grid method to measure sample size. Prior to stability testing, we placed each sample over a 0.5-cm grid (inset, Figure 3-2) and counted the number of squares that the sample covers (with a precision of ½ a square). After performing wet sieving, we counted the number of squares that the sample covered and divided by the original measurement to obtain the proportion remaining and assigned stability classes accordingly.

During data collection, we observed that biocrust samples reached the maximum soil stability class very quickly. Therefore, we expanded the stability classes from 6 to 9 and performed additional testing on all samples that were rated as class 6 during the initial testing. Using a protocol adapted from Belnap et al. 2008, we placed the remaining sample into a 20ml

sample tube and added 15ml distilled water. The samples were then shaken with a 90° elbow motion for 10 seconds at a rate of 2 forward-backward cycles per second. After shaking, the entire contents of the tube were poured over the sieve and the remaining proportion of the sample relative to the original sample size was recorded. We characterized stability classes 7-9 as described in table 3-1B, based on the methodology used in Belnap et al. (2008).

During field sample collection, the lighting conditions varied from day to day. To ensure consistent observations of biocrust development levels, we took a photograph of each sample accompanied by a white balance/exposure "grey card". After field data collection, all photographs were processed in Adobe Photoshop Lightroom (Adobe, San Jose, CA) photography software. Each photograph was manually adjusted for white balance and exposure using the grey card as a reference (Figure 3-3). This allowed for estimations for the varying of biocrust levels of development to be consistent between samples and across several days of field data collection.

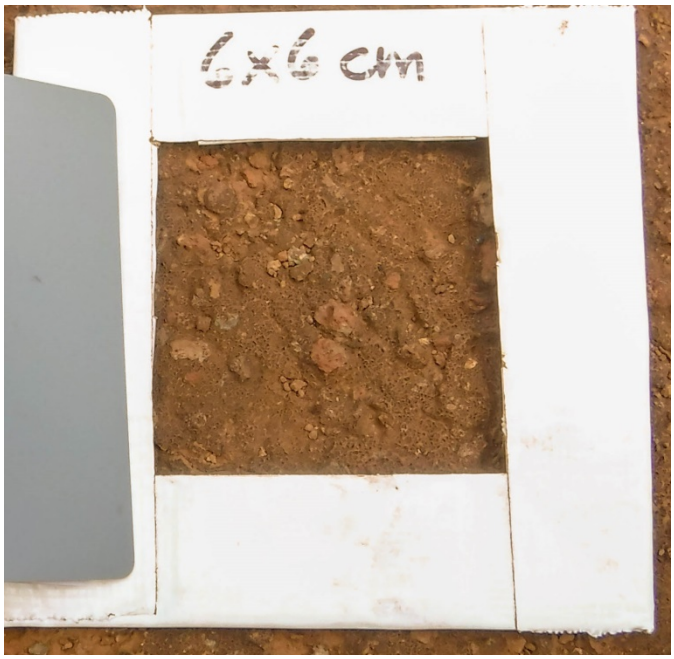

Figure 3-3: Photograph of biocrust sample for soil stability testing. Calibration grey card is shown at left.

3.23 Imagery collection and processing

For comparisons of soil loss over time, sUAS imagery was collected in January 2019 using the same calibration tarp and flight parameters as described in section 2.31. We also obtained data from a flight conducted in April 2016 using a Swinglet CAM fixed-wing platform (Sensefly, Lausanne, Switzerland) with a 16.8-megapixel Canon Powershot ELPH 110 HS camera (Canon, Tokyo, Japan). Prior to analysis, we verified that the spatial resolution between the two data sets was comparable: 3.01 cm/pixel for the 2016 flight and 2.84 cm/pixel for the 2019 flight. For each flight, raw imagery was processed using the same procedure described in section 2.31 to create a digital surface model (DSM) for elevation change analysis and an orthomosaic that was used for georectification.

To georeferenced each data set, we used a modified version of the methods outlined in section 2.14 using field-marked ground control points (GCPs) that were visible in both mosaics. After identifying GCPs from the mosaics we extracted horizontal positional data by creating points over each GCP in ArcMap v. 10.4, extracting the coordinates for each point, and geotagging images that contained those GCPs using Pix4D. This process generated mean RMSEs of 2.1 cm and 2.8 cm for the 2016 and 2019 flights, respectively. To further align the data sets with each other we used manual tie points which are created directly in a reference point cloud (in this case the 2019 DSM). Manual tie points were selecting using features (i.e., rocks) which appeared in both mosaics. We verified the vertical alignment of the two DSMs by selecting 25 "invariant" points (other rocks) scattered throughout the study site that were visible in both mosaics (Figure 3-4). At each of these points we calculated the elevation difference between the two DSMs and then calculated the mean of those values to determine the precision of the alignment. The invariant points showed considerable variation in elevation across the study site (mean DSM difference = 0.074 m, SD = 0.096 m), so we focused further analysis on a subsection of the site that had more consistent values at the invariant points. To verify to DSM differences within the subsection, we added an additional 10 invariant points (15 in total) which increased the mean difference between the DSMs (Table 3-2) but reduced the spread of the values (mean DSM difference = 0.15 m, SD = 0.032 m) so that we could consider the mean difference as an offset estimate in subsequent calculations of elevation change.

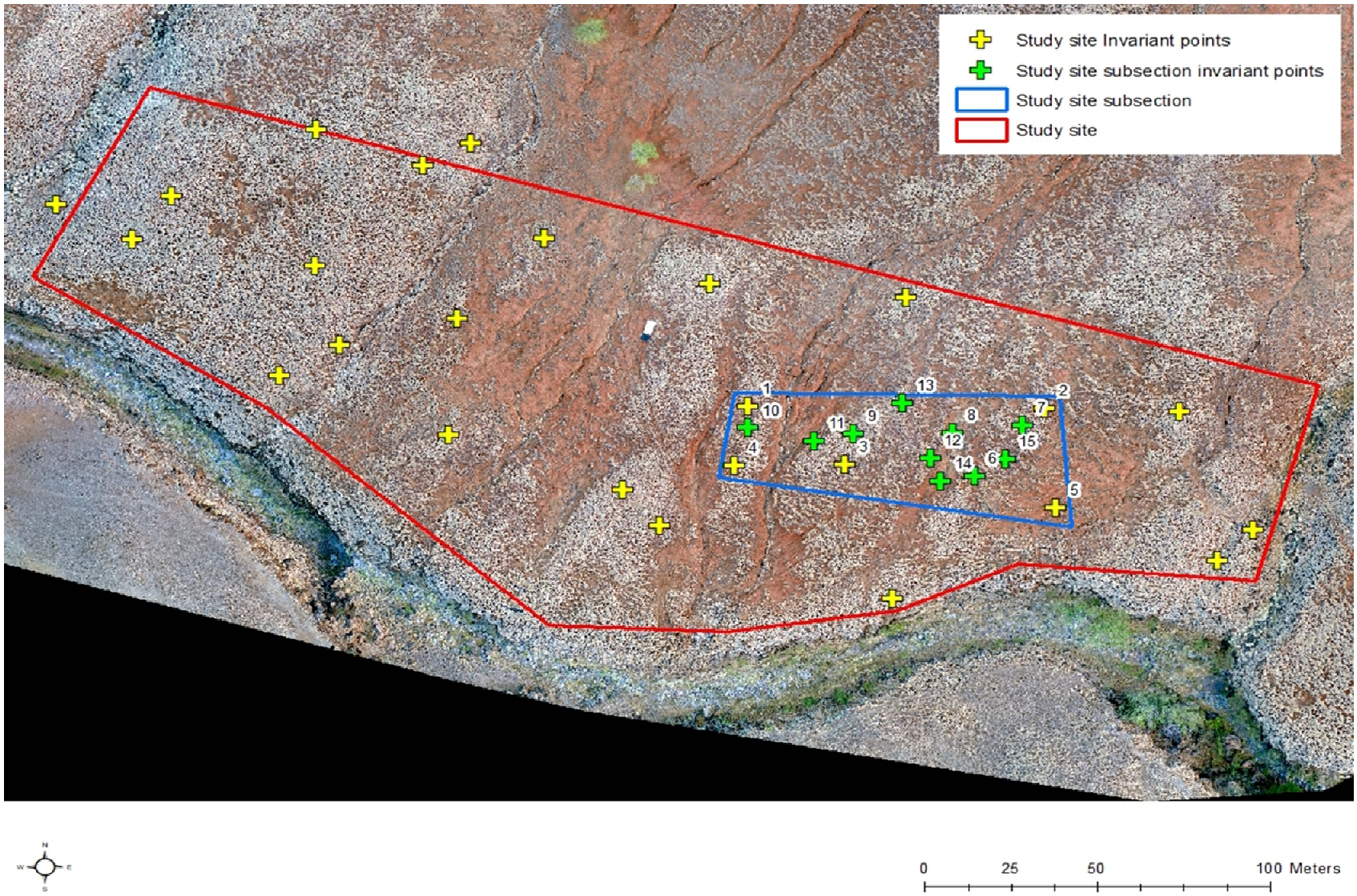

Figure 3-4: map of study area (outlined in red) and subsection (blue). Invariant points are shown with yellow (larger study area) and green (subsection) crosses.

Table 3-2: Values at each invariant point (corresponding to labels in Figure 3-4), obtained from subtracting the 2016 DSM from the 2019 DSM.

Invariant point	2019 DSM value (m)	2016 DSM value (m)	DSM difference (m) 2019-2016
1	385.1764	385.0201	0.1564
2	389.0447	388.8498	0.1618
3	391.5083	391.3435	0.1603
4	390.0252	389.9282	0.1555
5	384.2915	384.0901	0.1743
6	388.0188	387.9243	0.1477
7	386.0855	385.9265	0.0970
8	384.5837	384.4616	0.0945
9	386.4301	386.2593	0.1580
10	387.6223	387.5046	0.2006
11	384.3648	384.2061	0.1222
12	382.5447	382.3892	0.1709
13	386.4930	386.3452	0.2032
14	385.4112	385.2849	0.1270
15	385.4656	385.2930	0.1177
Mean			0.1498

For comparisons between grazed and non-grazed sites, sUAS imagery was collected in December 2018 at an altitude of 115 m AGL over the exclusion section and the adjacent grazing-accessible land using the same calibration tarp and flight parameters described in section 2.31. Raw imagery was processed and calibrated using the same procedure described in section 2.31, although GCPs were omitted because georectification was not necessary for this analysis.

3.24 Image classification

We classified the sUAS-derived mosaics slightly differently, depending on the research question (Figure 3-5). For estimating soil loss among different land cover types, we classified the 2019 orthomosaic using the step-wise method described in section 2.14 with the following three classes: vegetation ground cover, bare soil, and biocrust (the biocrust class encompassed only LODs 2-3 to maximize classification accuracy – see section 2.32). We also performed an

accuracy assessment prior to further analysis and determined overall accuracy (91.53%, kappa = 0.863) and class-specific producer and user accuracies (Table 3-3). We were able to conduct an accuracy assessment for all land cover types because the erosion study site overlapped the classification site from Chapter 2 so we had previously-groundtruthed training and validation data sets.

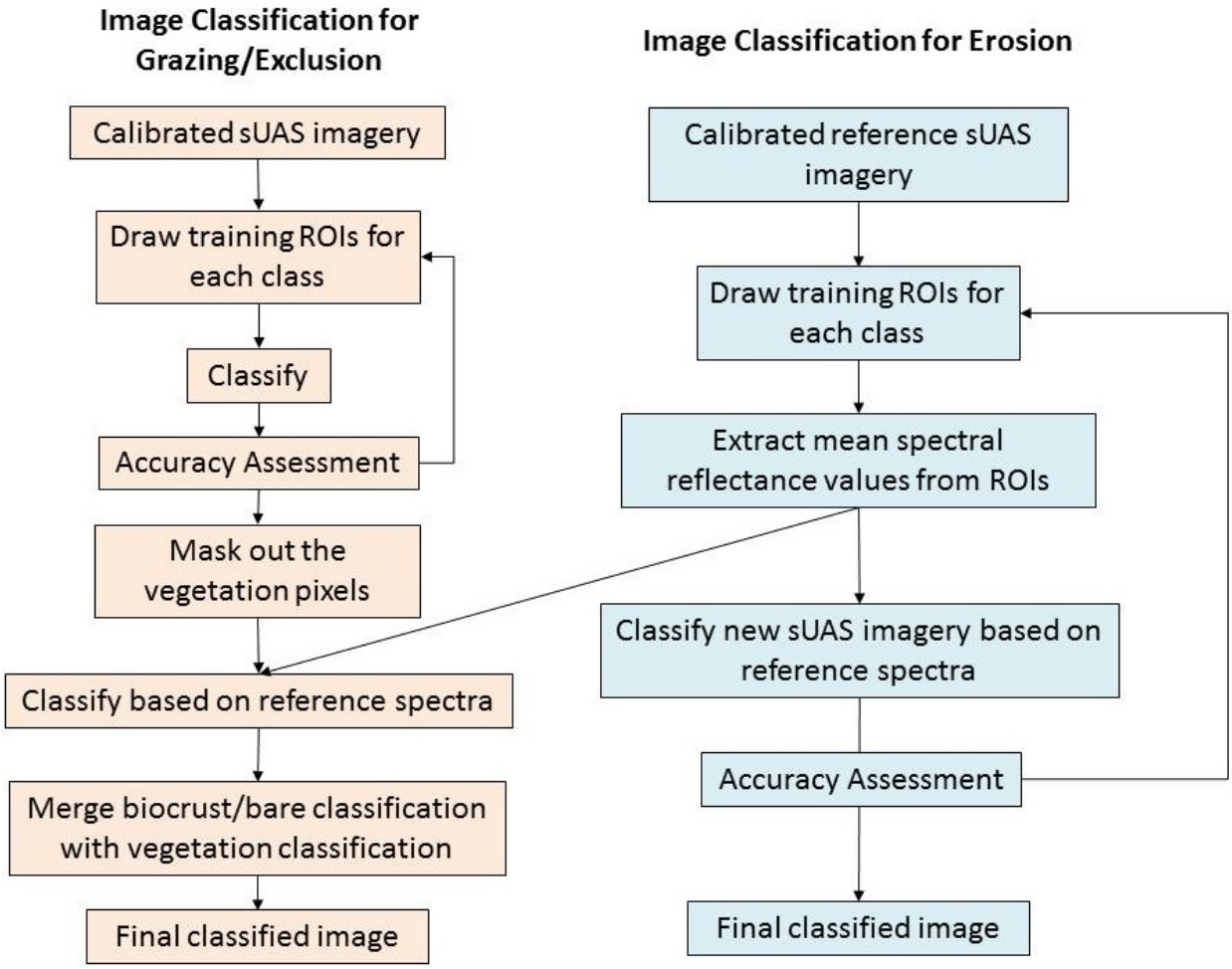

Figure 3-5: Workflow of image classification for grazing exclusion research question (left) and soil loss research question (right).

Table 3-3: Accuracy by land cover class for erosion-related image classification.

	Erosion classification	
Land cover type	Producer Accuracy	User Accuracy
Vegetation	96.42%	97.21%
Biocrust	84.18%	84.80%
Bare soil	88.54%	86.43%

For comparisons of the grazed and non-grazed site we used an approach that allowed us to avoid additional, resource-intensive groundtruthing. We created a preliminary classification of vegetation and non-vegetation areas and then masked out the vegetation pixels using the same methods outlined in section 2.14. We conducted accuracy assessments for the preliminary classification to determine overall accuracy (92.54%, kappa = 0.851) and class-specific accuracies (Table 3-4). After masking, we classified the non-vegetation pixels as either biocrust or bare soil using spectral endmembers derived from reference imagery that had been previously groundtruthed (see section 2.13). This classification approach identifies the spectral reflectance of reference ROIs and uses that data to classify to the imagery of interest (Adams et al. 1995). We obtained reference spectra from the flight conducted for erosion data collection in January 2019, when the vegetation condition was similar to the imagery collected in December 2018, so that the spectral data among the land cover classes would be consistent between the reference ROIs and the orthomosaic classified for grazing exclusion analysis. We used the accuracy assessment of the erosion image classification (see Table 3-3) as an approximation of accuracy for the grazing exclusion bare soil and biocrust classification.

Table 3-4: Classification accuracy of vegetation and ground land covers in grazing exclusion study site. *Ground class was further classified into bare soil and biocrust using endmember spectra.

	Grazing exclusion classification	
Land cover type	Producer Accuracy	User Accuracy
Vegetation	96.69%	89.07%
Ground*	88.53%	96.51%

3.25 Data analysis

All soil stability statistical analysis was performed using RStudio (www.r-project.org). Subsamples were pooled to give a final sample size of n=60 (n=12 per biocrust LOD). Histograms showed a non-normal data distribution, so we used the non-parametric Kruskal-Wallis test to find whether there was a difference between median soil stability at the varying biocrust levels of development. We also performed post-hoc pairwise Wilcox rank-sum testing with a Bonferroni p-value adjustment to compare soil stability between specific levels of development. To obtain numeric variables for statistical analysis, we used a value of -1 to represent loose, non-crusted soil while biocrust LOD 0-3 retained their numeric values.

All spatial data analysis was performed using ArcMap v. 10.4 and ENVI v. 5.3 software. To estimate soil loss, we measured elevation changes by subtracting the pixel values of the 2016 DSM from the values of the 2019 DSM:

$$Elevation\ change = T2 - T1$$

Equation 2: Calculation of elevation changes between 2016 and 2019, where T2 = 2019 DSM pixel values and T1 = 2016 DSM pixel values.

We then determined the elevation difference per land cover class by grouping the elevation change data set based on the classified land cover map and calculated descriptive statistics for elevation change in each class. To compare biocrust coverage in the grazing-accessible and exclusion sites, we generated study sites on the classified map by manually drawing an equal-sized polygon (4000 m^2) for each treatment. We calculated the area of each land cover type by multiplying the pixel count per class by the pixel size of the image (7.941×10^{-4} m^2/pixel).

3.3 Results

3.31 Relationship between biocrust development and soil stability

We found that there was a statistically significant difference ($p=1.73 \times 10^{-9}$, $\chi^2=46.74$, df=4) between median stability class among biocrusts at different levels of development. Higher development levels exhibited higher stability, although the relationship between development

level and soil stability was not linear (Figure 3-6). Our data were not normally distributed, so we were unable to perform an analysis of variance (ANOVA) but we found a general trend of lower variance in soil stability among the higher levels of development. From the pairwise comparisons, we found differences between some levels of development but not others. There was a significant difference in soil stability class between LOD -1 and all other LOD, and between LOD 0 and all other LOD. However, there was no significant difference in soil stability class between LODs 1, 2 and 3 (Table 3-5).

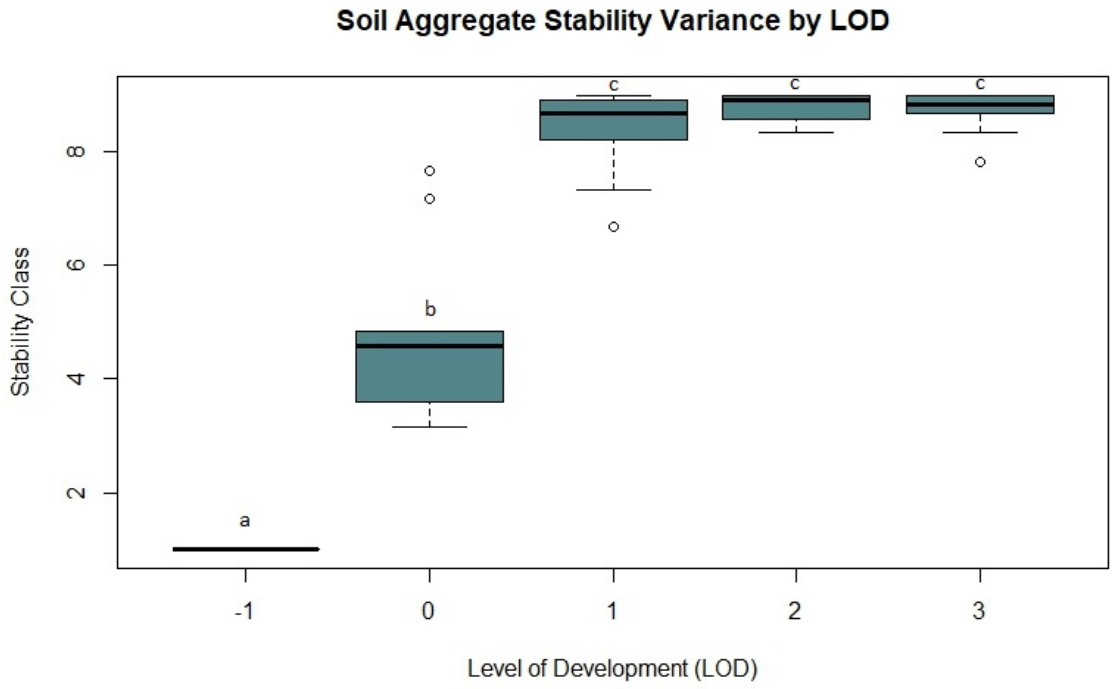

Figure 3-6: Boxplot of biocrust development level and associated soil stability. Different lowercase letters indicate significant differences in soil stability, based on pairwise comparisons.

Table 3-5: p-values from pairwise comparisons of soil stability class among varying levels of biocrust development.

LOD	-1	0	1	2
0	1.0×10^{-4}			
1	9.8×10^{-5}	7.3×10^{-4}		
2	8.5×10^{-5}	3.1×10^{-4}	1.0	
3	8.8×10^{-5}	3.2×10^{-4}	1.0	1.0

3.32 Elevation changes between April 2016 and January 2019

The analysis produced a map of varying elevation changes across the study area between 2016 and 2019 (Figure 3-7). A summary of changes between the 2016 and 2019 DSMs is presented in Table 3-6; prior to offset correction the bare soil and biocrust classes showed an increase in elevation. However, after subtracting the average offset (0.151 m, Table 3-4) we found that the bare soil class decreased 11.8 cm/pixel, while the biocrust class increased 22.7 cm/pixel.

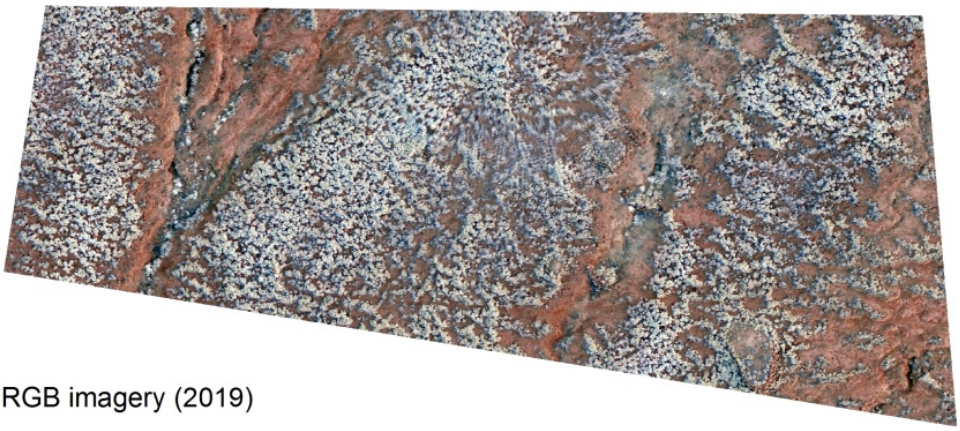

RGB imagery (2019)

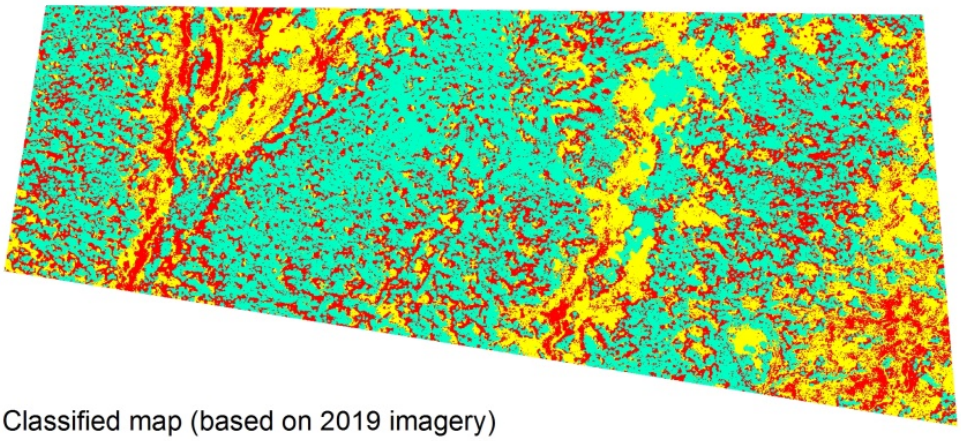

Classified map (based on 2019 imagery)

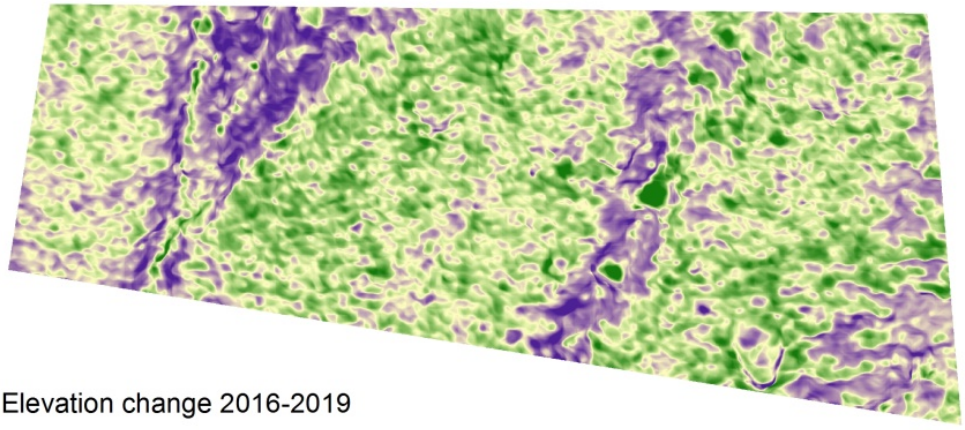

Elevation change 2016-2019

Figure 3-7: Land cover classifications in January 2019 and elevation changes between April 2016 and January 2019.

Table 3-6: Proportion of land area, raw elevation changes, and offset-corrected elevation changes within each land cover class. Error estimates are based on classification producer accuracies for each land cover.

Land cover class	Proportion of site area	Raw mean elevation change per pixel (cm)	Offset-corrected mean elevation change per pixel (cm)
Biocrust	27.8 ± 4.4%	17.4	2.3
Bare soil	23.8 ± 2.7%	13.9	-1.2
Vegetation	48.4 ± 1.7%	23.2	8.1

3.33 Biocrust cover in grazed and non-grazed sites

All of the land cover types showed different areas of coverage between the two treatments. In the exclusion site, vegetation was the dominant cover type, while in the grazed site the cover types were present in roughly equal proportions (Figure 3-8). Biocrusts had more coverage in the grazed site than the exclusion site: 38.6±6.1% and 17.8±2.8%, respectively (error estimates are based on producer accuracies for each land cover classification). Bare soil also had higher coverage in the grazed site (31.9±3.7%) than in the exclusion site (6.4±0.7%). Vegetation had substantially more coverage in the exclusion site (75.8±2.7%) than in the grazed site (29.5±1.1%).

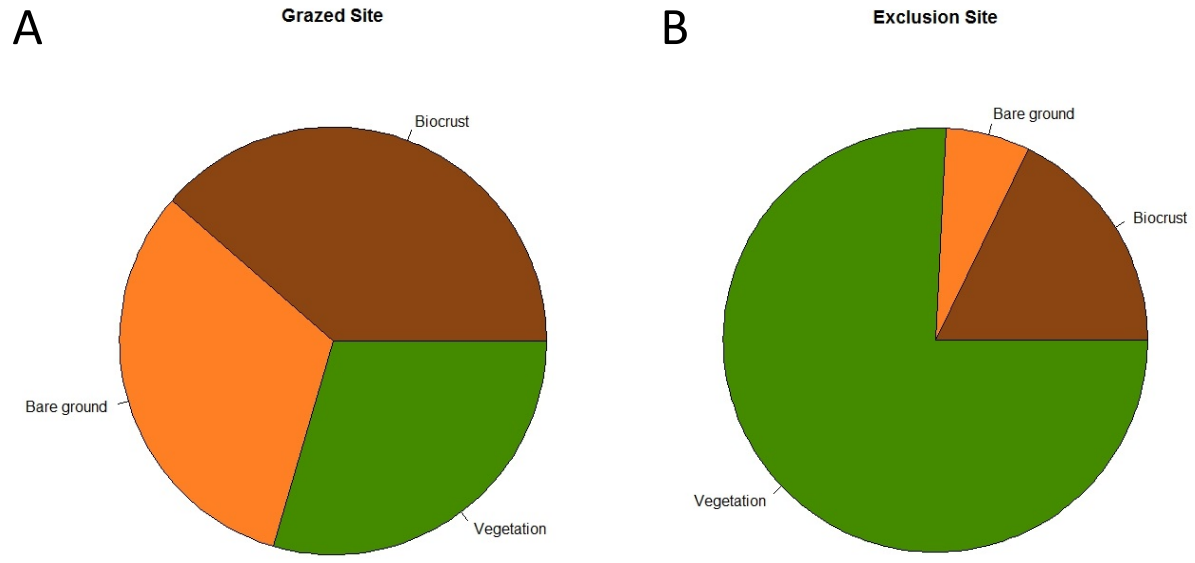

Figure 3-8: Area and proportion of land cover types in (A) grazed and (B) exclusion sites.

3.4 Discussion

3.41 Biocrust development and soil aggregate stability

As we had hypothesized, we found that soil stability increased with biocrust development level. Contrary to what we expected, however, we did not find a linear relationship between development and soil stability. Our positive association between biocrust development and soil stability is supported by previous research for biocrusts that are morphologically similar to those found at our study site (Issa et al. 2001, Belnap et al. 2008). However, those studies found significant differences in soil stability among varying development levels, which is not what our data showed. Our results indicated that there was a sharp increase between no visible biocrust and initial biocrust development (LOD 1), but that soil-stabilizing ability essentially plateaus beyond the initial biocrust development stage.

A possible explanation for our results may be the influence of soil characteristics. Previous research comparing biocrust development with soil aggregate stability was often conducted with biocrusts on sandy soils (Issa et al. 2001, Belnap et al. 2008). The sandy loam soils found in our study site, however, have higher clay content than sandy soils (Buol et al. 1997). Soils with more clay exhibit higher aggregate stability (Bissonais 1996) so it is possible that the soil's inherent stability obscured the differences among biocrust development levels. Also, sandy soil is coarse-textured, which negatively influences its ability to aggregate and thereby reduces stability (Brady 1974). So, it is possible that those previous studies found more significant differences in soil stability at different development levels because the underlying soil was inherently less stable. Further, the maximum LOD we observed in this study was 3; however, the LOD scale for biocrusts goes up to 6 (Belnap et al. 2008). Had our soils reached higher levels of development we might have found further increases in soil aggregate stability. Regardless, based on the substantial differences we found between soils with and without surface biocrusts, we conclude that biocrusts are actively stabilizing soils beyond the effects of soil composition or texture.

We also found a significant increase in aggregate stability between loose soils (LOD -1) and crusted soils that had no visible biocrusts (LOD 0). This may be a result of abiotic soil characteristics that promote soil aggregation, but could also be due to cyanobacteria that grow

below the soil surface and are difficult to see with the naked eye. Subterranean biocrust components (that move to the surface for photosynthesis when wet) contain similar filaments and exopolysaccharide excretions as their surface-dwelling counterparts and can also hold soil particles together (Colesie et al 2016). Although the soils at our study site may be more stable overall, these filaments could confer greater soil aggregate stability even if surface biocrusts are not present at the time of measurement. This reasoning is supported by the greater variability in stability class associated with LOD 0, which suggests that a factor beyond soil composition is influencing aggregate stability. Soil stability increases with biocrust abundance, in the form of biomass (Belnap et al. 2008), so we still expected to find lower stability in crusted soils without visible surface components and that is what our results reflect. Our field data were constrained to visible surface biocrusts because our research was also focused on biocrust mapping with visible-wavelength imagery (see chapter 2). The significant difference in soil stability that we found between LOD 0 and LOD 1-3, however, indicates that biocrust mapping can be limited to visible, surface biocrusts without risk of overlooking substantial soil-stabilizing development levels.

Our results suggest that biocrusts are important soil-stabilizers in the Kawaihae watershed. Considering the arid climate and limited water availability, the establishment of biocrusts which can thrive under these harsh conditions is beneficial to this landscape and to the aquatic communities harmed by soil inputs. Greater soil aggregate stability is associated with a lower susceptibility to erosion (Barthes & Roose 2002), suggesting that biocrusts which are allowed to develop on the surface undisturbed can improve the soil's stability and therefore confer greater erosion resistance than bare soil alone. Biocrusts may also support other restoration initiatives, such as out-planting of native plant species. Biocrusts play a role in capturing dew (Jing et al. 2009) and enhancing plant nutrient uptake (Harper & Belnap 2001), which is beneficial for both established plants and those acclimating from transplantation. Considering that biocrusts are already present within the watershed, protection of these communities would likely generate positive downstream effects for the entire ecosystem. Restoration of the Kawaihae watershed can even be extended to strategic colonization of exposed soils with cultivated biocrusts, which can be grown relatively rapidly in a greenhouse environment (Wang et al. 2009, Antoninka et al. 2014) and transferred to outdoor landscapes (Wang et al. 2009, Chiquoine et al. 2016). These transplanted biocrusts could have the benefit of

providing soil stabilization benefits without the high costs associated with the establishment and maintenance of traditional erosion-mitigation methods such as native out-planting and check dams.

Combined with biocrust spatial distribution data, our results can aid conservation efforts by providing a proxy for soil stability in non-vegetated patches based on biocrust presence or absence. While more research is needed, these data suggest that erosion mitigation methods such as native out-planting for increased vegetation cover and sediment check dams that prevent the movement of sediment downhill may be implemented more effectively by highlighting specific target areas that are lacking in biocrust cover and are therefore at higher risk of erosion. Approaching land management for conservation in this targeted fashion would save time and allow for a more efficient use of resources. Knowledge of the soil-stabilizing effects of biocrusts in a spatial context can also be useful for directing the movements of field crews so as to avoid harming the very landscape they are working to improve. For example, biocrust distribution maps can be used to demarcate trails for field crews who are checking fence lines, out-planting, etc. so that they avoid areas of biocrust growth. These considerations are particularly important because biocrusts lose their soil-stabilizing ability when they are trampled (Kuske et al. 2012), so progression towards conservation goals necessitates consideration of biocrusts when traversing the landscape.

3.42 Biocrusts and soil loss over time

As expected, based on visual differences between the 2019 and 2016 mosaics, vegetation height increased during the time period studied. Surprisingly, the height of soil (as measured from elevation change) also increased within the biocrust cover type. Although biocrusts are considered an important factor in soil accumulation due to their ability to capture dust (Williams et al 2012), it is unlikely that an average 0.03m/pixel of soil accumulated within only the biocrust-covered portion of the study site over the relatively short time span that we studied. It is more likely that there were alignment errors between the two DSMs used to estimate elevation change. Although substantial effort was made to align the DSMs, there was still variation even among the “invariant” points. Data from sUAS platforms have been shown to be comparable to other high-resolution data collections systems, such as Light Detecting and Ranging (LiDAR), for soil transport estimates (Kaiser et al. 2014, Eltner et al. 2015, Neugirg et al. 2015) but

considering our large elevation change values and the unconfirmed quality of the 2016 data set we are unable to confidently say that our sUAS-based measurements reflect real values on the ground. However, additional field work could be undertaken to verify the elevation changes observed in our data set. More accurate, field-measured GCPs would improve the alignment of the DSMs and terrestrial LiDAR data could be collected to verify the changes that we measured via the DSMs. Our results could also be compared with traditional field methods, such as erosion pins that measure soil loss over time (Haigh 1997). There are currently erosion pins within our study site, and we hope to access the data sets from this equipment in the future. This would provide empirical estimates of soil loss or gain that could verify our results or, if our results are contradicted by the field data, guide future erosion-related geospatial data collection.

The challenges associated with alignment of the two DSMs preclude reliable conclusions regarding specific soil change values. However, additional data collection may still verify the relative elevation changes that we observed among land cover types. We found a substantial difference in elevation changes between the biocrust and bare soil cover types, and much more negative elevation change in the bare soil cover than in the biocrust cover. Relative soil loss estimates are supported by the positive elevation change in the vegetation cover class between the DSMs. Vegetation is expected to increase in height over time, so the increase in elevation for the vegetation class indicates that the comparison of the DSMs is capturing at least some of the elevation change patterns in the way that one would expect. If the differences between the DSMs are indicative of real-life patterns of vertical change for vegetation, then it is possible that they are also realistically depicting the changes for bare soil and biocrusts. In addition, a visual comparison between the DSM differences and the 2019 mosaics provided in Figure 3-4 reveals that the distribution of sediment loss matches up with more bare surfaces and rills (surface grooves that run downhill, visible in purple in Figure 3-7) than vegetated areas. Erosion severity can be higher for rills than flat, exposed ground (Kimaro et al. 2008, Eltner et al. 2015), further supporting the idea that the patterns visible in our data may accurately reflect relative soil loss intensities across the study area even if the specific soil loss values are not reliable.

If our observations are verified by future field data, the relatively lower soil loss rate in the biocrust-covered areas would suggest that biocrusts are holding soils in place and preventing them from being transported, and even that they may be building soils. The positive relationship

between biocrust cover and soil stability is well-documented (Belnap & Eldridge 2001, Belnap 2006, Belnap et al 2008, Issa et al. 2001, Chaudary et al. 2016, Rodriguez-Caballero et al. 2018), and is further supported in the Kawaihae watershed by our research. Adding this direct measure of the impact of biocrust cover on erosion in the study area provides supporting evidence of the important role of biocrusts as an erosion-mitigating factor in the Kawaihae watershed. Knowledge of this previously-overlooked ecosystem component, combined with our highly-detailed data sets of other land cover types, could assist ranchers and conservationists in more efficiently managing the landscape for multiple services.

Field-verification of our results could also have implications for research on the influence of biocrusts on erosion. Field-based studies on the effects of biocrust cover on erosion rates have shown that areas without biocrust cover experience substantially more sediment loss than those that have biocrusts (Chamizo et al. 2017) and that higher biocrust development is associated with lower sediment loss (Barger et al. 2006). However, our research methods can potentially estimate sediment loss across a much larger area and without the need for time-consuming field work. If these initial results are verified, this methods could dramatically strengthen our spatially-explicit understanding of the link between the soil-stabilizing properties of biocrusts and erosion, as well as open the doors for further research into the spatial distribution of erosion and the influence of biocrust cover on multiple scales.

3.43 Biocrusts and grazing ungulates

Our results indicate that biocrust coverage is influenced by the presence of grazing ungulates in the study area, but not in the way that we had expected. Vegetation cover followed the expected pattern, with higher coverage in the exclusion site than in the grazed site. Similarly, there was more bare ground in the grazed site than in the exclusion site. Contrary to what we had predicted, the absolute cover of biocrust was higher in the grazed site than in the exclusion site (Figure 3-8). If we consider the space available for biocrust colonization, however, we see substantial differences between relative biocrust cover in the grazed and exclusion sites. In the grazed site, the non-vegetated areas were a roughly 50/50 ratio of biocrust and bare soil. In the exclusion site the ratio of biocrust to bare soil is closer to 75/25, indicating that biocrusts have colonized a larger proportion of the available area in the exclusion site.

We used the endmember method to distinguish between bare soil and biocrusts in the non-vegetated areas by way of reference spectra, but it necessary to note that this classification method does not include groundtruthed data sets for these land cover types. The ~1:1 ratio of bare ground cover to biocrust cover that we found in the grazed site is similar to groundtruthed classifications we performed in a nearby site also accessible to grazing animals (see section 2.31). However, our research would benefit from groundtruthing biocrust and bare soil to verify the results presented here.

Our results must also be interpreted within the context of our study site. For example, grazing at our site may not high be high enough to affect biocrust cover as dramatically as in areas where grazing is more intensive. Previous studies have found that biocrusts exhibit variable growth at different levels of grazing intensity (Thomas & Dougill 2007, Concostrina-zubiri et al. 2013, 2014). However, definitions of grazing intensity levels are often inconsistent among studies, making direct comparisons difficult (Belnap & Eldridge 2001) and the different types of ungulates present in the paddock (cows and goats) have variable effects on soils (Eldridge et al. 2017). In addition, the rotational grazing style used in the Kawaihae watershed complicates estimations of grazing pressure. Further research in these areas would help us to understand how grazing pressure has influenced our results and how grazing effects the interactions between vascular plants and biocrusts in our island ecosystems.

The timespan of grazing exclusion may also influence the land cover patterns we found. Our exclusion site was chosen opportunistically, so we were limited to a single replicate that was fenced from grazers for ~10 years. Biocrust recovery after disturbance can vary according to localized climate, soil, and disturbance characteristics (Belnap & Eldridge 2001) and the recovery patterns of the biocrust communities at our exclusion site are not currently known. Biocrust growth rates have not been documented within the Kawaihae watershed or other drylands in Hawai'i, and further study in this subject area could clarify the timing of biocrust recovery following the removal of grazing.

Vegetation was the dominant land cover in the exclusion site and left only ~25% of the site exposed and thus available for biocrust growth. By comparison, ~70% of the grazed site was available for biocrusts. The disparate proportions of biocrust cover across open spaces in grazed vs. exclusion sites indicates that grazing animals are having a negative impact on biocrust

abundance. Because plants are taking up so much more of the surface area when grazing is excluded, and because plants can outcompete biocrusts for sunlight, it makes sense that the overall cover of biocrusts (and bare ground) would decline. Further, although the total cover of biocrusts declines with grazing exclusion, the proportion of biocrusts relative to bare ground increases dramatically, suggesting that less of the soil not covered by plants would be at highest risk for erosion.

The presence of biocrusts may have even promoted further plant growth by providing nutrients to the soil (Rodriguez-Caballero et al. 2018) and increasing nutrient uptake (Harper & Belnap 2001), thus furthering plant growth in the exclusion space. Despite the resulting reduction in space available for biocrusts, the biocrusts which are present may be providing additional benefits to this landscape as it recovers from grazing disturbance. In this way, increases in plant cover and the increased proportion of biocrust cover versus bare ground may both be increasing the stability of soils in the exclusion site.

Aside from covering a larger portion of the available space, biocrusts in the exclusion site are also potentially more developed than those in the grazed site. Our classification method created a single biocrust class and did not differentiate between varying levels of development, so we do not know the extent of development at either site. It is possible, therefore, that the overall coverage of biocrust is higher in the grazed site but that the development level is lower. Trampling breaks apart biocrusts but does not necessarily cause mortality (Kuske et al. 2012), allowing for re-growth once protected from further disturbance. Re-growth of damaged biocrusts would facilitate development in the exclusion site to higher levels than biocrusts that are still under chronic disturbance in the grazed site. We omitted classifications of individual biocrust development levels because of the inability of our remote sensing classification scheme to accurately differentiate between varying levels of development (see section 2.51). We also omitted biocrust types, such as mosses and lichens, which are indicative of more progressed development and which, at least in other systems, provide very high stabilization to soils. We did not create classes for these biocrust types because they were not observed at adjacent field sites and a cursory, informal inspection of the grazing exclusion site did not reveal them to be present. This reveals an important limitation of the supervised classification approach, which is that it only considers classes that are user-defined. If the algorithm is not trained to look for a biocrust

type then it won't classify it as such even if it is present on the ground. From our results we cannot definitively say whether biocrust types indicative of advanced stages of development are present in the exclusion area. Our study could be extended to include development levels, and our initial results could be verified, with other remote sensing techniques or field-based surveys of biocrust types. Deeper knowledge of biocrust development in grazed and non-grazed sites would provide more details to land managers about the time span needed for biocrust recovery in this watershed, as well as a more nuanced understanding of the influence of grazing animals on biocrust growth.

Further research may support our findings, which would present several important considerations for conservation in the Kawaihae watershed. If biocrusts cover a larger proportion of the non-vegetated space when grazing animals are excluded, then grazing animals are causing impacts on the landscape that was previously known. Considering the multitude of ecosystem services that biocrusts provide, any effects on biocrusts from grazing animals could alter the function of the entire landscape. Understanding the effects of grazing on biocrusts can also be used to support management decisions and restoration in the watershed. From our data collection, we are now aware of the coverage of these beneficial communities when they are in a protected site. The services that biocrusts provide, such as soil stabilization and the promotion of plant growth, further exemplifies the importance of their protection as part of an overall restoration strategy.

Chapter 4: Conclusions

Historical land use patterns in the Kawaihae watershed have caused significant erosion with far-reaching effects. In addition to the impacts from soil loss on the terrestrial landscape, the adjacent marine ecosystem of Pelekane Bay has been significantly damaged by sediment deposition from the upslope landscape (DeMartini et al. 2013, Stender et al. 2014, Takesue & Storlazzi 2019) and important native Hawai'ian cultural sites have also been buried by sediment entering the bay (Cheney et al. 1997, Cochran et al. 2016). The impacts from erosion in the watershed are so pervasive that it is important to look beyond traditional mitigation approaches and take advantage of less-obvious soil stabilization factors. Biocrusts have the potential to play an important role in reducing sediment transport in the Kawaihae watershed, but up until now there has been no data on biocrust distribution in any of the Hawai'ian Islands.

In this thesis, we present the first research into biocrust distribution on the Big Island. We have developed a novel mapping methodology for biocrusts using commercially-available sUAS platforms with cameras operating within visible wavelengths. We have integrated this data collection approach with well-established image processing and classification techniques to produce highly accurate and precise classified maps of biocrust distribution. Because of the accessibility of our approach, my methods can be applied to biocrusts in other parts of Hawai'i as well as other landscapes around the world. Using this methodology, other researchers could explore the spatial dimensions of biocrust growth over larger areas than would be feasible with traditional field methods, while still maintaining a high level of detail. This opens the door to research on larger-scale patterns of various biocrust metrics such as patchiness, edge effects and patch distribution. Our remote sensing approach can also be applied to places where biocrusts have been under-studied, which has been identified as a highly-important research topic (Weber et al. 2016). For example, sUAS platforms could be used to conduct exploratory surveys in areas that are likely candidates for biocrust colonization, based on local landscape and climate characteristics, and potential biocrust patches could be identified and groundtruthed using the same methods that we discuss in this thesis. This approach would be more efficient than traditional field-based methods for finding biocrusts, such as hiking transects, and has the added benefit of avoiding disturbance.

In addition to the development of a mapping methodology, we present the first research on the relationship between biocrust development and soil stability in the Hawai'ian Islands, specifically the Kawaihae watershed. Our research shows that biocrusts enhance soil stability in the watershed and that any stage of surface development confers higher resistance to breakdown than exposed soil alone. Soils that contain biocrusts are therefore less likely to be transported by erosive forces towards Pelekane Bay, providing benefits to the marine ecosystems of west Hawai'i as well as the terrestrial landscape. Our research provides insight into a previously-overlooked factor influencing erosion in Kawaihae watershed, which broadens our understanding of soil dynamics within this landscape.

Based on our findings, biocrusts should be taken into consideration during future restoration activities in the Kawaihae watershed. Biocrust distribution data could be incorporated when planning activities that involve moving people and equipment across the landscape. Conservation agencies could also consider cultivation and out-planting of biocrusts as an additional restoration strategy. Although additional feasibility analysis would be necessary and although research on biocrust out-planting is still underway, inoculating sites with biocrusts may provide a substantial benefit at less cost than planting and irrigating individual grasses and shrubs. Future erosion modelling for the watershed should also consider biocrusts when parameterizing land cover types. There are models such as the Rangeland Hydrology and Erosion Model (RHEM), which incorporates biocrust cover and is optimized for use in drylands (Nearing et al. 2001), that could be applied to the Kawaihae watershed to generate a more accurate analysis of erosion risk. Erosion modelling could also include the very high-spatial resolution data sets that we generated during the course of this research. These data sets would allow for predictions of sediment loss at small spatial scales, which could aid in restoration initiatives such as construction of sediment check dams.

Because of data collection and analysis limitations, some of our findings are more appropriately considered preliminary results. Biocrusts may directly influence soil loss over time, but challenges with aligning two different spatial data sets prevents me from drawing concrete conclusions surrounding the specific soil loss values that we obtained. Similarly, the presence of grazing animals may have a significant impact on biocrust growth in the Kawaihae watershed, but image classification accuracies and site-specific considerations limit the

confidence that we have in our results. However, in both cases we have observed trends that may be verifiable through additional research. We hope to further explore the initial patterns that we've seen in this research by collecting more accurate geospatial data with aerial and/or land-based systems in conjunction with additional field data.

In addition to supporting conservation in Hawai'i, this thesis expands the biocrust knowledge base. Biocrust research has so far been mostly limited to continental regions (Bowker et al. 2016). Our research provides insights on biocrusts in an island landscape that is also extremely geographically isolated, promoting further exploration of biocrust dispersal patterns and evolutionary trends. Previous research on biocrusts in an island ecosystem, San Nicholas Island off the coast of California, resulted in the description of nine new species of cyanobacteria and algae (Fletchner et al. 2008). Considering the geography and evolutionary history of the Hawai'ian Islands, there is a high possibility of future research leading to the discovery of additional new species which would, in turn, further our knowledge of biocrusts worldwide. Biocrusts have been referred to as "diminutive communities of global importance" (Ferrenberg et al. 2017). We encourage other researchers to explore the role that biocrusts play in conservation of Hawai'ian drylands and to further investigate Hawai'ian biocrusts within the context of general biocrust research.

References

Adams, John B., Milton O. Smith, Raimundo Almeida Filho, Valerie Kapos, Donald E. Sabol, Dar A. Roberts, and Alan R. Gillespie. 1995. "Classification of Multispectral Images Based on Fractions of Endmembers: Application to Land-Cover Change in the Brazilian Amazon." *Remote Sensing of Environment* 52 (2): 137–54.

Afek, Yehuda, and Ariel Brand. 1998. "Mosaicking of Ort Horectified Aerial Images." *Photogrammetric Engineering & Remote Sensing* 64 (2): 115125.

Anderson, Karen, and Kevin J. Gaston. 2013. "Lightweight Unmanned Aerial Vehicles Will Revolutionize Spatial Ecology." *Frontiers in Ecology and the Environment*.

Antoninka, Anita, Matthew A. Bowker, Sasha C. Reed, and Kyle Doherty. 2016. "Production of Greenhouse-Grown Biocrust Mosses and Associated Cyanobacteria to Rehabilitate Dryland Soil Function." *Restoration Ecology*.

Barger, Nichole N., Jeffrey E. Herrick, Justin Van Zee, and Jayne Belnap. 2006. "Impacts of Biological Soil Crust Disturbance and Composition on C and N Loss from Water Erosion." *Biogeochemistry*.

Barthes B, Roose E. 2002. Aggregate stability as an indicator of soil susceptibility to runoff and erosion ; validation at several levels. Catena **47**:133–149.

Baugh, W. M., and D. P. Groeneveld. 2008. "Empirical Proof of the Empirical Line." *International Journal of Remote Sensing* 29 (3): 665–72.

Belnap, J., and D. Eldridge. 2001. "Disturbance and Recovery of Biological Soil Crusts." In *Biological Soil Crusts: Structure, Function and Management*, 363–83. https://doi.org/10.1007/978-3-642-56475-8_27.

Belnap, Jayne. 2006. "The Potential Roles of Biological Soil Crusts in Dryland Hydrologic Cycles." *Hydrological Processes* 20 (15): 3159–78. https://doi.org/10.1002/hyp.6325.

Belnap, Jayne, Bettina Weber, and Burkhard Büdel. 2016. "Biological Soil Crusts as an Organizing Principle in Drylands." Page 3-14 in B. Weber, B. Budel, and J. Belnap, editors. Biological Soil Crusts: An Organizing Principle in Drylands.

Belnap J, Gardner J. 1993. Soil microstructure in soils of the Colorado Plateau: the role of the cyanobacterium Microcoleus vaginatus. Western North American Naturalist **53**:40–47.

Belnap J, Phillips SL, Witwicki DL, Miller ME. 2008. Visually assessing the level of development and soil surface stability of cyanobacterially dominated biological soil crusts. Journal of Arid Environments **72**:1257–1264.

Belnap J, Rosentreter R, Leonard S, Kaltenecker J, Williams J, Eldridge D. 2001. Biological soil crusts: ecology and management. US Dept. of Interior Technical Report: 1730–2.

Belnap J. 2003. The world at your feet: desert soil crusts. Frontiers in Ecology and Environment **1**:181–189.

Bissonnais, Y Le, and D Arrouays. 1996. "Aggregate Stability and Assessment of Soil Crustability and Erodibility: I. Theory and Methodology." *European Journal of Soil Science* 47 (4): 425–37. https://doi.org/10.1111/j.1365-2389.1996.tb01843.x.

Bowker MA, Belnap J, Bala Chaudhary V, Johnson NC. 2008. Revisiting classic water erosion models in drylands: The strong impact of biological soil crusts. Soil Biology and Biochemistry **40**:2309–2316.

Bowker MA, Belnap J, Davidson DW, Goldstein H. 2006. Correlates of biological soil crust abundance across a continuum of spatial scales: Support for a hierarchical conceptual model. Journal of Applied Ecology **43**:152–163.

Bowker MA, Maestre FT, Mau RL. 2013. Diversity and Patch-Size Distributions of Biological Soil Crusts Regulate Dryland Ecosystem Multifunctionality. Ecosystems **16**:923-933.

Brady NC. 1974. Organic matter of mineral soils. In: *The nature and properties of soils*, 137-163. Macmillan Publishing Co., New York.

Budel B, Dulic T, Darienko T, Rybalka N, Friedl T. 2016. Cyanobacteria and algae of Biological Soil Crusts. Page 55-80 in B. Weber, B. Budel, and J. Belnap, editors. Biological Soil Crusts: An Organizing Principle in Drylands.

Buol SW, Hole FD, McCracken RJ, Southard RJ. 1997. Soil Genesis and Classification. Iowa State University Press.

Chamizo, Sonia, Emilio Rodríguez-Caballero, José Raúl Román, and Yolanda Cantón. 2017. "Effects of Biocrust on Soil Erosion and Organic Carbon Losses under Natural Rainfall." *Catena* 148: 117–25. https://doi.org/10.1016/j.catena.2016.06.017.

Chaudhary, V. Bala, Matthew A. Bowker, Thomas E. O'Dell, James B. Grace, Andrea E. Redman, Matthias C. Rillig, and Nancy C. Johnson. 2016. "Untangling the Biological Contributions to Soil Stability in Semiarid Shrublands." *Ecological Applications* **19** (1): 110–22. https://doi.org/10.1890/07-2076.1.

Chen J, Ming YZ, Wang L, Shimazaki H, Tamura M. 2005. A new index for mapping lichen-dominated biological soil crusts in desert areas. Remote Sensing of Environment **96**:165–175.

Cheney DP, Hemmes DE, Nolan R. 1977. Puukohola Heiau National Historic Site Marine Fauna. Technical Report #13. Honolulu, HI

Chiquoine, Lindsay, Scott Abella, and Matthew Alan Bowker. 2016. “Rapidly Restoring Biological Soil Crusts and Ecosystem Functions in a Severely Disturbed Desert Ecosystem.” *Ecological Applications* 4 (26): 1260–72. https://doi.org/10.1002/15-0973.

Chuvieco, Emilio. 2016. *Fundamentals of Satellite Remote Sensing: An Environmental Approach*. 2nd ed. Boca Raton: Taylor & Francis Group.

Cochran SA, Gibbs AE, Logan JB. 2006. Geologic Resource Evaluation of Pùukohola – Heiau National Historic Site,Hawaìi Part II: Benthic Habitat Mapping Scientific Investigations Report 2006-5254. Honolulu, HI

Colesie C, Felde VJMNL and Büdel B. 2016. Composition and macrostructure of biological soil crusts. Page 159-172 in B. Weber, B. Budel, and J. Belnap, editors. Biological Soil Crusts: An Organizing Principle in Drylands.

Concostrina-Zubiri, L., E. Huber-Sannwald, I. Martínez, J. L. Flores Flores, and A. Escudero. 2013. “Biological Soil Crusts Greatly Contribute to Small-Scale Soil Heterogeneity along a Grazing Gradient.” *Soil Biology and Biochemistry*. https://doi.org/10.1016/j.soilbio.2013.03.029.

Concostrina-Zubiri L, Huber-Sannwald E, Martínez I, Flores Flores JL, Reyes-Agüero JA, Escudero A, Belnap J. 2014. Biological soil crusts across disturbance-recovery scenarios: Effect of grazing regime on community dynamics. Ecological Applications **24**:1863–1877.

Cook KL. 2017. An evaluation of the effectiveness of low-cost UAVs and structure from motion for geomorphic change detection. Geomorphology **278**:195–208.

Crosby MR. 1965. New Records for Hawaiian Island Mosses. The Bryologist **68**:457–462.

DeMartini E, Jokiel P, Beets J, Stender Y, Storlazzi C, Minton D, Conklin E. 2013. Terrigenous sediment impact on coral recruitment and growth affects the use of coral habitat by recruit parrotfishes (F. Scaridae). Journal of Coastal Conservation **17**:417–429.

Department of Health, State of Hawaii. 2014. 2014 State of Hawaii Water Quality Monitoring and Assessment Report **303**:1–124. Honolulu, HI.

Duffy JP, Pratt L, Anderson K, Land PE, Shutler JD. 2018. Spatial assessment of intertidal seagrass meadows using optical imaging systems and a lightweight drone. Estuarine, Coastal and Shelf Science **200**:169–180.

Eldridge, David J., Manuel Delgado-Baquerizo, Samantha K. Travers, James Val, and Ian Oliver. 2017. “Do Grazing Intensity and Herbivore Type Affect Soil Health? Insights from a Semi-Arid Productivity Gradient.” *Journal of Applied Ecology*.

Eltner, Anette, Philipp Baumgart, Hans Gerd Maas, and Dominik Faust. 2015. "Multi-Temporal UAV Data for Automatic Measurement of Rill and Interrill Erosion on Loess Soil." *Earth Surface Processes and Landforms*. https://doi.org/10.1002/esp.3673.

Ferrenberg S, Tucker CL, Reed SC. 2017. Biological soil crusts: diminutive communities of potential global importance. Frontiers in Ecology and the Environment:1–8.

Fischer T, Subbotina M. 2014. Climatic and soil texture threshold values for cryptogamic cover development: a meta-analysis. Biologia (Poland) **69**:1520–1530.

Fisher, Jonathan R.B., Eileen A. Acosta, P. James Dennedy-Frank, Timm Kroeger, and Timothy M. Boucher. 2017. "Impact of Satellite Imagery Spatial Resolution on Land Use Classification Accuracy and Modeled Water Quality." *Remote Sensing in Ecology and Conservation* 4 (2): 137–49. https://doi.org/10.1002/rse2.61.

Garaba, Shungudzemwoyo Pascal, Jan Schulz, Marcel Robert Wernand, and Oliver Zielinski. 2012. "Sunglint Detection for Unmanned and Automated Platforms." *Sensors (Switzerland)* 12 (9): 12545–61. https://doi.org/10.3390/s120912545.

Giambelluca TW, Chen Q, Frazier AG, Price JP, Chen Y-L, Chu P-S, Eischeid JK, Delparte DM. 2013. Online Rainfall Atlas of Hawai'i. Bulletin of the American Meteorological Society **94**: 313-316.

Gomes I, Peteiro L, Bueno-Pardo J, Albuquerque R, Perez-Jorge S, Oliviera ER, Alaves FL, Queiroga H. "What's a Picture Really Worth? On the Use of Drone Aerial Imagery to Estimate Intertidal Rocky Shore Mussel Demographic Parameters." *Estuarine, Coastal and Shelf Science* 213 (April): 185–98. https://doi.org/10.1016/j.ecss.2018.08.020.

Graef, F., and K. Stahr. 2000. "Incidence of Soil Surface Crust Types in Semi-Arid Niger." *Soil and Tillage Research* 55 (3–4): 213–18. https://doi.org/10.1016/S0167-1987(00)00117-3.

Greene LW. 1993. A Cultural History of Three Traditional Hawaiian Sites on the West Coast of Hawai'i Island. U.S. Department of the Interior, National Park Service, Denver Service Center.

Grishkan, Isabella, and Giora J. Kidron. 2013. "Biocrust-Inhabiting Cultured Microfungi along a Dune Catena in the Western Negev Desert, Israel." *European Journal of Soil Biology* 56: 107–14. https://doi.org/10.1016/j.ejsobi.2013.03.005.

Haigh MJ. The use of erosion pins in the study of slope evolution. British Geomorphological Research Group Technical Bulletin. 1977(18):31-49

Harper, Kimball T., and Jayne Belnap. 2001. "The Influence of Biological Soil Crusts on Mineral Uptake by Associated Vascular Plants." *Journal of Arid Environments*. https://doi.org/10.1006/jare.2000.0713.

Herrick, JE, WG Whitford, AG de Soyza, JW Van Zee, KM Havstad, CA Seybold, and M Walton. 2001. "Field Soil Aggregate Stability Kit for Soil Quality and Rangeland Health Evaluations." *Catena* 44: 37–35.

Issa, O, Bissonnais Y, Defarge C, and Trichet J. 2001. "Role of a Cyanobacterial Cover on Structural Stability of Sandy Soils in the Sahelian Part of Western Niger." *Geoderma* 101: 15–30.

Zhang J, Zhang Y, Downing A, Cheng J, Zhou X, and Zhang B. 2009. "The Influence of Biological Soil Crusts on Dew Deposition in Gurbantunggut Desert, Northwestern China." *Journal of Hydrology* 379 (3–4): 220–28. https://doi.org/10.1016/j.jhydrol.2009.09.053.

Jorge-Villar SE, Edwards HGM. 2008. Lichen colonization of an active volcanic environment: A Raman spectroscopic study of extremophile biomolecular protective strategies. Journal of Raman Spectroscopy **41**:63–67.

Kaiser A, Neugirg F, Rock G, Müller C, Haas F, Ries J, and Schmidt J. 2014. "Small-Scale Surface Reconstruction and Volume Calculation of Soil Erosion in Complex Moroccan Gully Morphology Using Structure from Motion." *Remote Sensing*. https://doi.org/10.3390/rs6087050.

Karnieli A. 1997. Development and implementation of spectral crust index over dune sands. International Journal of Remote Sensing **18**:1207–1220.

Karnieli A, Kokaly RF, West NE, Clark RN. 2001. "Remote Sensing of Biological Soil Crusts." Pages 432-455 in B. Weber, B. Budel, and J. Belnap, editors. Biological Soil Crusts: An Organizing Principle in Drylands.

Kelcey, J., and A. Lucieer. 2012. "Sensor correction and radiometric calibration of a 6-band multispectral imaging sensor for uav remote sensing." *ISPRS - International Archives of the Photogrammetry, Remote Sensing and Spatial Information Sciences*.

Kidd C, Mcgregor G. 2007. Observation and characterisation of rainfall over Hawaii and surrounding region from the Tropical Rainfall Measuring Mission **27**:541–553.

Kimaro DN, Poesen J, Msanya BM, Deckers JA. 2008. "Magnitude of Soil Erosion on the Northern Slope of the Uluguru Mountains, Tanzania: Interrill and Rill Erosion." *Catena*. https://doi.org/10.1016/j.catena.2008.04.007.

Kuske CR, Yeager CM, Johnson S, Ticknor LO, Belnap J. 2012. Response and resilience of soil biocrust bacterial communities to chronic physical disturbance in arid shrublands. ISME Journal **6**:886–897. Nature Publishing Group.

Lal R. 2004. Soil carbon sequestration to mitigate climate change. Geoderma **123**:1-22.

Laliberte et al. 2007),

Laliberte AS, Herrick JE, Rango A, Winters C. 2010. “Acquisition, Orthorectification, and Object-Based Classification of Unmanned Aerial Vehicle (UAV) Imagery for Rangeland Monitoring.” *Photogrammetric Engineering & Remote Sensing* **76** (6): 661–72.

Latty RS, Hoffer RM. 1981. “Computer-Based Classification Accuracy Due to the Spatial Resolution Using Per-Point Versus Per-Field Classification Techniques.” Proceedings of the seventh international symposium on machine processing of remotely sensed data with special emphasis on range, forest and wetlands assessment. http://docs.lib.purdue.edu/lars_symphttp://docs.lib.purdue.edu/lars_symp/448.

Lim, YS, Phu HL, Jong SP, Lee MH, Pyeon MW, Kim JL. 2015. “Calculation of Tree Height and Canopy Crown from Drone Images Using Segmentation.” *Journal of the Korean Society of Surveying, Geodesy, Photogrammetry and Cartography* **33** (6): 605–14. https://doi.org/10.7848/ksgpc.2015.33.6.605.

López-Granados F, Torres-Sánchez J, Serrano-Pérez A, de Castro AI, Mesas-Carrascosa FJ, Peña JM. 2016. Early season weed mapping in sunflower using UAV technology: variability of herbicide treatment maps against weed thresholds. Precision Agriculture **17**:183–199.

Maestre FT, Escolar C, de Guevara ML, Quero JL, Lázaro R, Delgado-Baquerizo M, Ochoa V, Berdugo M, Gozalo B, Gallardo A. 2013. Changes in biocrust cover drive carbon cycle responses to climate change in drylands. Global Change Biology.

Mafanya M, Tsele P, Botai J, Manyama P, Swart B, Monate T. 2017. Evaluating pixel and object based image classification techniques for mapping plant invasions from UAV derived aerial imagery: Harrisia pomanensis as a case study. ISPRS Journal of Photogrammetry and Remote Sensing **129**:1–11.

Meron E, Yizhaq H, Gilad E. 2007. Localized structures in dryland vegetation: Forms and functions. Chaos **17**(3):037109.

Michez A, Piégay H, Lisein J, Claessens H, Lejeune P. 2016. Classification of riparian forest species and health condition using multi-temporal and hyperspatial imagery from unmanned aerial system. Environmental Monitoring and Assessment **188**:146.

Moss B, We OC, Bay P, Restoration W. 2011. Pelekane Bay Watershed Restoration Project : 16 months later | Hawaii247 . com.

Munsell AH. A color notation. Munsell color company; 1919.

Munsell Color 1994. Munsell soil color charts, revised edition. Munsell Color Company, New Windsor, NY

Soil Survey Staff, Natural Resources Conservation Service, United States Department of Agriculture. Official Soil Series Descriptions. Available online. Accessed [03/10/2019].

Nearing MA et al. 2005. Modeling response of soil erosion and runoff to changes in precipitation and cover. Catena **61**:131-154.

Neugirg F, Kaiser A, Schmidt J, Becht M, Haas F. 2015. Quantification, analysis and modelling of soil erosion on steep slopes using LiDAR and UAV photographs. IAHS-AISH Proceedings and Reports **367**:51–58.

Noy-Meir I. 1973. Desert Ecosystems: Environment and Producers. Annual Review of Ecology and Systematics **4**:25-51.

Oceanit Center 2007. Pelekane Bay Watershed Sediment Runoff Analysis. Honolulu, HI.

Ortega-Terol D, Hernandez-Lopez D, Ballesteros R, Gonzalez-Aguilera D. 2017. Automatic hotspot and sun glint detection in UAV multispectral images. Sensors (Switzerland).

Peña JM, Torres-Sánchez J, Serrano-Pérez A, de Castro AI, López-Granados F. 2015. Quantifying efficacy and limits of unmanned aerial vehicle (UAV) technology for weed seedling detection as affected by sensor resolution. Sensors **15**:5609-5626.

Polyakov VO, Nichols MH, McClaran MP, Nearing MA. 2014. Effect of check dams on runoff, sediment yield, and retention on small semiarid watersheds. Journal of Soil and Water Conservation **69**:414–421.

Quinton J, Govers G, Van Oost K, Bardgett R. The impact of agricultural soil erosion on biogeochemical cycling. Nature Geoscience **3**:311.

Rodríguez-Caballero E, Cantón Y, Chamizo S, Lázaro R, Escudero A. 2013. Soil Loss and Runoff in Semiarid Ecosystems: A Complex Interaction Between Biological Soil Crusts, Micro-topography, and Hydrological Drivers. Source: Ecosystems **16**:529–546.

Rodríguez-Caballero E, Escribano P, Cantón Y. 2014. Advanced image processing methods as a tool to map and quantify different types of biological soil crust. ISPRS Journal of Photogrammetry and Remote Sensing **90**:59–67.

Rodríguez-Caballero E, Cantón Y, Jetten V. 2015. Biological soil crust effects must be included to accurately model infiltration and erosion in drylands: An example from Tabernas Badlands. Geomorphology **241**:331–342.

Rodríguez-Caballero E, Escribano P, Olehowski C, Chamizo S, Hill J, Cantón Y, Weber B. 2017. Transferability of multi- and hyperspectral optical biocrust indices. ISPRS Journal of Photogrammetry and Remote Sensing **126**:94–107.

Rodríguez-Caballero E, Chamizo S, Roncero-Ramos B, Román R, Cantón Y. 2018. Runoff from biocrust: A vital resource for vegetation performance on Mediterranean steppes. Ecohydrology **11**:1–13.

Rosentreter R, Bowker M, Belnap J. 2007. A Field Guide to Biological Soil Crusts of Western U.S. Drylands - Common Lichens and Bryophytes. U.S. Government Printing Office, Denver, Colorado.

Rozenstein O, Adamowski J. 2017. A review of progress in identifying and characterizing biocrusts using proximal and remote sensing. International Journal of Applied Earth Observation and Geoinformation **57**:245–255.

Sala OE, Lauenroth WK. 1982. Small rainfall events: An ecological role in semiarid regions. Oecologia **53**:301-04.

Sato HH, Ikeda W, Paeth R, Smythe R, Takehiro M. 1973. Hawaii Island Soil Survey. United State Department of Agriculture, Hilo, HI.

Seppelt RD, Downing AJ, Deane-Coe KK, Zhang Y, Zhang J. 2016. Bryophytes within biological soil crusts. Page 101-120 in B. Weber, B. Budel, and J. Belnap, editors. Biological Soil Crusts: An Organizing Principle in Drylands.

Shao G, Wu J. 2008. On the accuracy of landscape pattern analysis using remote sensing data. Landscape Ecology **23**:505-511.

Smith GM, Milton EJ. 1999. The use of the empirical line method to calibrate remotely sensed data to reflectance. International Journal of Remote Sensing **20**:2653–2662.

Smith CW. 1981. Bryophytes and Lichens of the Puhimau Geothermal Area , Hawaii Volcanoes National Park. The Bryologist **84**:457–466.

Staples GW, Imada CT, Hoe WJ, Smith CW. 2004. A revised checklist of Hawaiian mosses. Bryophyte Diversity and Evolution **25**:36.

Stender Y, Jokiel PL, Rodgers KS. 2014. Thirty years of coral reef change in relation to coastal construction and increased sedimentation at Pelekane Bay, Hawai‘i. PeerJ **2**:300.

Stewart MC. 2005. Pelekane Bay Watershed Management Plan. South Kohala, Hawaii Mauna Kea Soil and Water Conservation District Pelekane Bay Watershed Management Plan-2005.

Takesue RK, Storlazzi CD. 2019. Geochemical sourcing of runoff from a young volcanic watershed to an impacted coral reef in Pelekane Bay, Hawaii. Science of the Total Environment **649**:353–363. Elsevier B.V.

Teillet PM, 1986. Image correction for radiometric effects in remote sensing. International Journal of Remote Sensing **12**:1637-51.

Thomas AD, Dougill AJ. 2007. Spatial and temporal distribution of cyanobacterial soil crusts in the Kalahari: Implications for soil surface properties. Geomorphology **85**:17-29.

Timm O, Diaz HF. 2009. Synoptic-statistical approach to regional downscaling of IPCC twenty-first-century climate projections: Seasonal rainfall over the Hawaiian Islands. Journal of Climate **22**:4261–4280.

Tissot B. 1998. Changes in the Marine Habitat and Biota of Pelekane Bay , Hawai ' i Over a 20-Year Period. U.S. Fish and Wildlife Service, Honolulu, HI.

Tonkin TN, Midgley NG, Graham DJ, Labadz JC. 2014. The potential of small unmanned aircraft systems and structure-from-motion for topographic surveys: A test of emerging integrated approaches at Cwm Idwal, North Wales. Geomorphology **226**:35–43.

Torres-Sánchez J, Peña JM, de Castro AI, López-Granados F, 2014. Multi-temporal mapping of the vegetation fraction in early-season wheat fields using images from UAV. Computers and Electronics in Agriculture **1**(103):104-13.

Turner D, Lucieer A, Watson C. 2012. An automated technique for generating georectified mosaics from ultra-high resolution Unmanned Aerial Vehicle (UAV) imagery, based on Structure from Motion (SFM) point clouds. Remote Sensing **4**:1392–1410.

Turner MG, Dale VH, Gardner RH. 1989. Predicting across scales: Theory development and testing. Landscape Ecology **3**:245–252.

Turner D, Lucieer A, Wallace L. 2014. Direct georeferencing of ultrahigh-resolution UAV imagery. IEEE Transactions on Geoscience and Remote Sensing **52**(5):2738-2745.

Vallet J, Panissod F, Strecha C, Tracol M. 2011. Photogrammetric Performance of an Ultra Light Weight Swinglet "Uav." ISPRS - International Archives of the Photogrammetry, Remote Sensing and Spatial Information **39-1/C22**:253–258.

Ventura D, Bruno M, Jona G, Belluscio A. 2016. Estuarine , Coastal and Shelf Science A low-cost drone based application for identifying and mapping of coastal fi sh nursery grounds. Estuarine, Coastal and Shelf Science **171**:85–98.

Verity GE, Anderson DW. 1990. Soil erosion effects on soil quality and yield. Canadian Journal of Soil Science **70**:471–484.

von Bueren SK, Burkart A, Rascher U, Hueni A, Yule IJ, Tuohy MP. 2015. Deploying four optical UAV-based sensors over grassland: challenges and limitations. Biogeosciences **12**:163-175.

Wang C, Myint SW. 2015. A Simplified Empirical Line Method of Radiometric Calibration for Small Unmanned Aircraft Systems-Based Remote Sensing. IEEE Journal of Selected Topics in Applied Earth Observations and Remote Sensing.

Wang W, Liu Y, Li D, Hu C, Rao B. 2009. Feasibility of cyanobacterial inoculation for biological soil crusts formation in desert area. Soil Biology and Biochemistry **41**:926–929. Elsevier Ltd. Available from http://dx.doi.org/10.1016/j.soilbio.2008.07.001.

Weber B, Cantón Y, Rodríguez-Caballero E, Olehowski C, Escribano P, Chamizo S, Hill J. 2017. Transferability of multi- and hyperspectral optical biocrust indices. ISPRS Journal of Photogrammetry and Remote Sensing **126**:94–107.

Wei Wei, Liding Chen, Bojie Fu. 2009. Effects of rainfall change on water erosion processes in terrestrial ecosystems: a review. Progress in Physical Geography **33**:307–318.

Westoby MJ, Brasington J, Glasser NF, Hambrey MJ, Reynolds JM. 2012. "Structure-from-Motion" photogrammetry: A low-cost, effective tool for geoscience applications. Geomorphology **179**:300–314.

Williams AJ, Buck BJ, Beyene MA. 2012. Biological Soil Crusts in the Mojave Desert, USA: Micromorphology and Pedogenesis. Soil Science Society of America Journal.

Yu Q, Gong P, Clinton N, Biging G, Kelly M, Schirokauer D. 2006. Object-based detailed vegetation classification with airborne high spatial resolution remote sensing imagery. Photogrammetric Engineering & Remote Sensing **72**:799–811.

Zhao Y, Xu M. 2013. Runoff and soil loss from revegetated grasslands in the hilly Loess Plateau region, China: Influence of biocrust patches and plant canopies. Journal of Hydrologic Engineering **18**:387–393. Available from http://www.scopus.com/inward/record.url?eid=2-s2.0-84881332461&partnerID=40&md5=3ce69aeda69fe8442c8287c20b80dfa9.